RSC Advances

ROYAL SOCIETY OF CHEMISTRY

www.rsc.org/advances

Structures and morphologies of biocompatible and biodegradable block copolymers

Shaoyong Huang‡, Shichun Jiang†*

† School of Materials Science and Engineering, Tianjin University, Tianjin 300072, P. R. China;

‡ Key Laboratory of Polymer Eco-materials, Changchun Institute of Applied Chemistry, Chinese Academy of Sciences, Changchun 130022, P. R. China

* Corresponding author: scjiang@tju.edu.cn

Abstract: Biocompatible and biodegradable block copolymers (BBCPs) become increasingly important in polymer science, and have great potential applications in polymer materials. Structures of BBCPs, which are determined by the competition between crystallization, microphase separation, kinetics and processing, have a tremendous influence on the final properties and applications. In this review, the most recent advances are highlighted in the crystalline structures and morphologies of BBCPs with at least one crystalline block. Particular emphasis is place on the influences of chemical composition, molecular architecture, crystallization pathway, and film thickness on structures and morphologies of the block copolymers. The formation and the characters of the structures grown in the block copolymers are helpful for understanding the interplay between crystallization and phase segregation, morphologies, structural evolution and their applications.

Keywords: Block copolymer; biocompatible and biodegradable; crystalline structure; morphology; microphase separation

1. Introduction

Block copolymers with biodegradability and biocompatibility have attracted more and more attention because of potential applications in environmentally friendly and medical fields [1-11]. The block copolymers are an interesting option, which combinations of different chemical structures can be employed without macroscopic phase segregation [3, 12, 13]. Most of the biocompatible and biodegradable polymers are semi-crystalline, such as poly(L-lactic acid) (PLLA), poly(D-lactic acid) (PDLA), poly(ethylene oxide) or poly(ethylene glycol) (PEO or PEG),

poly(ε-caprolactone) (PCL), poly(p-dioxanone) (PPDX), poly(propene glycol) (PPG), poly(hydroxyl butyrate) (PHB), poly(butylene succinate) (PBS), poly(3-hydroxyalkanoate) (PHA), and poly(glycolic acid) (PGA). Usually, three kinds of block copolymers including AB diblock, ABA triblock and multi-arm block copolymers have been synthesized and investigated. Structures and morphologies of these block polymers resulting from crystallization and microphase separation determine the final properties, such as biodegradability, biocompatibility, optical and mechanical properties, by dominating microstructure, micro-domain morphology and overall crystallinity [14-18].

The blocks in block copolymers are usually immiscible and would undergo microphase separation under certain conditions [19, 20], which drives molecular chains to self-assemble into a variety of ordered nanostructures, including lamellae, spheres, cylinders and gyroids, depending on its chemical composition and thermal pathway [21-29]. The formation of these nanostructures is useful for the fabrication of functional materials, which can be applied in lithography, nanomaterials and opto-electronic devices [30-34]. The Crystal thickness of a semi-crystalline block copolymer usually is in the range of nanoscale. The size is comparable with the dimension of the micro-domains induced by microphase separation of block copolymers. Therefore, the block copolymers exhibit considerable morphology richness, arising from the two main forces that can drive structure development: microphase separation between the blocks, which favors the formation of nano-domains, and the crystallization of the blocks, which favors the formation of

alternating amorphous and crystalline layers [1].

Most of the biocompatible and biodegradable polymers are crystallizable. Consequently, the biocompatible and biodegradable block copolymers are usually consisting of at least one crystalline block. Therefore, the resulting structures formed by the block copolymers depend on the location of the order-disorder transition temperature (T_{ODT}), the glass transition temperature of the non-crystalline block (T_g) and the crystallization temperature (T_c) of the crystalline block. When the melting temperature of one block is much higher than the other block, such as PLLA-PCL and PLLA-PEG block copolymers, either crystallization can overwrite any previous micro-domains formed by microphase separation for weakly segregated systems or homogeneous systems, or crystallization can be confined within the micro-domains for strongly segregated systems [35-39]. For example, for crystallization of PLLA block in weakly segregated PLLA-PCL block copolymer, $T_{ODT} > T_c > T_g$, the initial crystallization occurs within the PLLA-rich micro-domains, and then the further crystallization breaks out the micro-domains, and a new structure is obtained driven by the crystallization of PLLA. In the same block copolymer, for the crystallization of PCL block, $T_{ODT} > T_g > T_c$, the crystallization of PCL block is confined in the micro-domains formed by microphase separation of the copolymer, crystallization and vitrification of PLLA block. When the melting temperatures of the two blocks in the copolymer are near enough, such as some PCL-PEO block copolymers, the situation can be even complicated, since the crystallization of one block and the structure formed can affect those of the other block. Moreover, a coincident

crystallization phenomenon of both blocks may be obtained in some PEG-PCL block copolymers [40-42].

In the present paper, the influences of chemical composition, molecular architecture, crystallization pathway, and film thickness on the structures of biocompatible and biodegradable block copolymers with at least one crystallizable block were reviewed.

2. Structures of biodegradable and biocompatible block copolymers (*BBCPs*)

2.1 Crystallization of miscible *BBCPs*

The structure of block copolymers is strongly depending on the chemical composition and crystallization kinetics. Based on the miscibility of the unlike blocks, the block copolymers can be generally clarified into weakly segregated and strongly segregated ones. There are two typical crystallization modes of polymer melting crystallization: break-out crystallization and confined crystallization. When the blocks of the block copolymers are weakly segregated, break-out crystallization will take place and lamellar structures with alternating crystalline-amorphous layers are usually formed [17, 18, 43-46]. The lamellar crystalline structures have been observed in the structures of PLLA-PEO or PLLA-PEG [15-18, 47-54], PEO-PCL or PEG-PCL [55-61], and PLLA-PCL diblock and triblock copolymers [62-64]. When the blocks are strongly segregated, the crystallization of the minor component may be confined in micro-domains driven by microphase separation.

Moreover, the crystalline structure of block copolymers is related to the fraction of each block and the relationship between three characteristic temperatures, T_{ODT} of

the order-disorder transition temperature, T_g of the non-crystalline block, and T_c of the crystalline block. Generally, if the weight fraction of the minor component is lower than 20%, it will be difficult to crystallize [17, 51, 55-58, 61, 65-67]. The crystallization of the crystallizable block will overwrite or be confined in the micro-domains, depending on the T_g of the non-crystalline component and the T_c of the crystallizable component. Break-out crystallization take place with $T_c > T_g$, and crystallization is confined for block copolymers with $T_g > T_c$ within 1D-, 2D- and 3D- corresponding to lamellar, cylindrical, and spherical micro-domains [68].

The melting point (T_m) and the crystallization temperature (T_c) of PLLA are ca. 160-180 ℃ and ca. 100~120 ℃, respectively. The T_c of PLLA is higher than the T_g of PEO, PCL, and part of other biocompatible and biodegradable polymers. In *BBCPs* containing PLLA major segment, the PLLA crystallization drives microphase separation and would break-out the previously formed micro-domains[1, 15-18]. Spherulitic morphologies have been reported in *BBPCs*, e.g. PLLA-PEO, PLLA-PCL, PEO-PCL, PPDX-PCL block copolymers. Morphologies changed with composition and crystallization pathway, due to the interaction of microphase separation and crystallization process. Figure 1 shows the morphologies of PLLA-PEO block copolymer driven by microphase separation and crystallization of PLLA. Spherulites were observed in low T_c range (at 90 ℃and 100 ℃ in Figure 1 (a) and (b)). Ring-banded spherulites were formed at higher T_cs (at 110 ℃ and 115 ℃ in Figure 1 (c) and (d)). An transitional morphology of which the center is spherulite and the outer is dendrite was observed at 115 ℃ (Figure 1 (d)). At T_cs

above 120 ℃, dendritic super-structures were formed as shown in Figure 1 (e) and (f). The angle between the second branch and the main branch was less than 90º in Figure 1 (e), while at 125 ℃ in Figure 1 (f), the angle between the second (third) branch and the main (second) branch was almost 90º, indicating the influence of micro-domains of microphase separation driven by crystallization and PEO/PLLA segregation.

The morphological evolution with crystallization pathway (T_c) can be schematically illustrated in Figure 2, which is associated with the microphase separation induced micro-domains and the break-out crystallization of PLLA block. With disorder to order transition, PEO-rich micro-domains and PLLA-rich micro-domains could be formed [1, 17, 18, 52, 69, 70]. Crystallization of PLLA starts in the PLLA-rich domains, because there are sufficient PLLA chains for initial growth of PLLA crystals .With consumption of the amorphous PLLA segments inside, the neighbor PLLA chains begin to diffuse onto the growth fronts, and break-out crystallization occurs. Because of the miscibility or weak segregation between PLLA and PEO blocks, amorphous PEO is rejected from PLLA crystalline lamellae, and distributed between PLLA lamellae and/or confined amorphous PLLA nano-domains [69-71]. At low T_cs, crystallization of PLLA determined the final morphologies, and spherulitic structures are produced. At high T_cs, phase separation induces single crystal formation [17, 52, 72], and dendritic morphologies are obtained. The morphological evolution with T_c is also seen in block copolymers of PLLA-PCL, PCL-PEO (or PCL-PEG), PPDX-PCL [15-18, 34-72].

The structural evolution may be related with different chain folding modes. Chain folding in block copolymers is a function of segregation strength of the unlike blocks [73], molecular weight of the crystalline block [74], and the crystallization temperature [75]. Generally, polymer chains tend to fold parallel to the copolymer interphases as shown in Figure 3a, when the block copolymers are strongly segregated, or the molecular weight of the crystalline block is small, or at low crystallization temperature ranges. Chain folding becomes perpendicular to the copolymer interphase as shown in Figure 3b, when the block copolymers are weakly segregated, or the molecular weight of the crystalline block is large, or at high crystallization temperature ranges. The nano-structural evolution of the biodegradable block copolymers is helpful for applications in nanotechnology [76-78].

In crystalline-amorphous and crystalline-crystalline *BBCPs*, one crystalline block crystallizes and break-out the microphase separation induced micro-domains. The mode of microphase separation induced micro-domains would influence the final structure of the block copolymers. Figure 4 shows the final morphologies of crystalline-amorphous PLLA30k-PEO5k block copolymer (30k and 5k correspond the molecular weight of each block). It is difficult for PEO5k to crystallize in PLLA30k-PEO5k block copolymer, because the volume fraction of PEO chains and the size of PEO-rich domains are too small to crystallize. Hexagonal and two peculiar dendritic morphologies are observed in PLLA30k-PEO5k block copolymers at high T_cs (120 and 130 ℃). In Figure 4a, there are two different sectors arranged

alternately, which can be classified in terms of the crystal growth direction and chain-folding [1, 17]. In Figure 4b and 4c, S-shaped structures are obviously seen, which is associated with two different growth modes of flat-on and edge-on, and the micro-domains formed by microphase separation and crystallization [17, 72, 69, 79].

2.2 Confined crystallization of *BBCPs*

Confined crystallization is usually observed in strong segregated or crystalline/glassy block copolymers [80-84], and some crystalline-crosslinking rubbery block copolymers [85]. The interface between the two immiscible micro-domains or the glassy wall of the glassy block have strong confinement on the crystalline block.

Figure 5 shows the atomic force microscopy images of double crystalline LA505EG505 (PLLA-PEG) diblock copolymer. The confined crystallization of single crystals was investigated. The crystallization process becomes more complicated in double crystalline block copolymers. The crystallization of LA505 takes place firstly, and the structures determined by microphase separation and crystallization of LA505 are vitrified by the glass transition of LA505. The crystalline and the glassy amorphous LA505 domains have strong confinement on crystallization of EG505. Actually, both blocks of LA505 and EG505 affect the crystallization behavior. The foregoing crystallization behavior of the PLLA severely constrains the crystallization of the PEG as shown the structures in Figure 5.

Hexagonal shaped PLLA single crystals, which are the same as PLLA homopolymer, grow firstly from PLLA-rich micro-domains, as shown in Figure 5a.

At the early stage of PLLA crystallization, microphase separation of PLLA/PEG blocks has little effect on the nanoscale crystalline structures of PLLA, but the further crystallization of PLLA is influenced by microphase separation. As a result, the LA505 lamellar crystal of the nether layer on the substrate is star-shaped, which is different from the single crystal of PLLA homopolymer, indicating its growth is affected by the nano-domains of EG505 block and microphase separation driven by simultaneous crystallization. The growth rate of the first layer is much higher than that of the second layer and the third layer crystal, due to sufficient amorphous PLLA blocks and the short diffusion length. After the crystallization of PLLA completes, the film is cooled to 35 °C for the crystallization of EG505 block. PLLA crystals acts as nuclei of PEG block (EG505), and PEG crystals emerge at the edge of PLLA crystals, as shown in Figure 5d. The final morphology of the LA505EG505 block copolymer changes into dendritic crystals because of the crystallization of the PEG block, as shown in Figure 5e and 5f. Crystallization of PLLA and microphase separation make PEG phase form nano- and micro-domains between PLLA crystal lamellae, the interfaces of polymer/air and polymer/substrate, and the bundles of PLLA crystals [1, 17, 18, 27, 29, 51-54, 69, 70].The crystallization of PEG block is confined by the glassy PLLA, and the crystal of PEG block grows epitaxially on the PLLA crystal. The (1 0 4) plane of the PEG crystal is parallel to the (0 0 1) plane of the PLLA crystal and the substrate [69].

Figure 6 shows the confined crystallization in symmetric PLLA-PEG block copolymer (LA5kEG5k) via two steps crystallization. At the beginning of 110 °C,

microphase separation has been absence after disorder to order transition. When the sample isothermally crystallized at 110 °C, only the PLLA component crystallize, and a dendritic morphology is observed as shown in Figure $6a_1$, $6a_1'$, or $6b_1$.The PEG component is still in molten state at 110 °C. On the one hand, the melted PEG block is in favor of PLLA crystallization, due to decreasing PLLA melt viscosity. On the other hand, the nanoscale and microscale domains of PEG suppress PLLA crystallization. In the crystallization process of PLLA block, the amorphous PEG block is eliminated from the growth front of PLLA crystals, resulting in nanoscale domains of PEG block. The crystallization of PLLA block induces a new segregated structure, which breaks up the previous structure formed by disorder to order transition of the block copolymer. When the PLLA-PEG block copolymer subsequently crystallize at 30 °C, PEG blocks started to crystallize, and a grain-like brighter area appear at the boundary of the foregoing PLLA spherulites (as shown in Figure $6a_2$ and $6a'_2$, marked by the circle). The brighter area finally covers the whole PLLA spherulite, as shown in Figure $6a_2$−$6a_4$, $6a_2'$−$6a_4'$, $6b_2$−$6b_4$. The PEG crystals grow in the regions of interlamellar of PLLA crystals confirmed by SAXS data, and fill into the amorphous spaces inside the PLLA spherulites [70]. Though PEG blocks crystallize in the block copolymer, morphological feature of the block copolymer do not change at all on the micrometer scale, as shown in Figure $6a_1$-$6a_4$ and $6b_1$-$6b_4$. However, the crystallization of PEG blocks significantly enhances the contrast of the foregoing PLLA spherulites by changing the optical property of the block copolymer, and it affects the structure in nanometer scale.

The spherical, lamellar and cylindrical micro-domains formed by microphase separation and/or the forgoing crystallization confine the crystallization of the second crystalline component. It should be noted that, although the morphology of the crystallized block copolymer is the same before and after confined crystallization, the properties, such as optical, mechanical, rheological and biodegradable properties [69, 86-88], are indeed altered due to the crystallization.

Both break-out and confined crystallization can be utilized to regulate the structure and properties of BBCPs, via controlling chemical composition, molecular weight, crystallization kinetics.

2.3 Eutectic crystal of double crystalline *BBCPs*

In weakly segregated block copolymers, eutectic structure can be obtained if the two different crystalline blocks have comparable T_cs and T_gs, because of the connectivity of the blocks in molecular level [14, 28, 40-42, 55-59, 65-67, 84-89]. In crystalline-crystalline PCL-PEG (or PCL-PEO) block copolymers, PEO and PCL lamellae occupy the same crystallites when comparable fractions of each component were present [14, 40-42, 84, 89]. Jiang et al. observed the ring-banded spherulite of the crystalline-crystalline PEO-PCL diblock copolymer with minor weight fraction of PEO block of 0.18. It is found that the PCL blocks crystallize firstly, and PEO blocks subsequently crystallize. PEO block crystallize in a soft-confinement, and concentric circles are not observed due to the minority fraction of PEO block [14]. With weight fraction of PEO component of ~0.40 and ~0.5, a unique double concentric spherulite can be obtained in PCL-PEO block copolymers [14, 40-42, 84,

90], as shown in Figure 7. He et al. used temperature-dependent FTIR to analyze the crystallization process of PEG-PCL [40]. It is found that the PCL block melted later in the heating process and crystallized firstly in the slow cooling process. Consequently, PCL spherulites are firstly observed, as shown in Figure 7a, and the growth rate of PCL is ca. 2.8 μm/s. Just after several seconds, a sudden birefringent change (marked by arrows in Figure 7b) within one spherulite is observed, and the growth rate of the new birefringence within the spherulite was 15.1 μm/s. The new birefringence triggered the growth of a new outer spherulite from the existing front of the inner spherulite (Figure 7c and 7d), resulting in a concentric spherulite. It is confirmed by in situ micro-beam FT-IR that the new outer spherulite is PEG, and the growth rate of PEG is 4.4μm/s. The decrease of the growth rate from 15.1μm/s to 4.4 μm/s indicates the soft confinement on crystallization of PEG blocks.

Moreover, the crystallization behavior and structure of PEO-b-PCL are significantly composition dependent. Figure 8 shows the time resolved SAXS and WAXS measurements of PEO-PCL block copolymers collected during the isothermal crystallization at 40 ℃. In the copolymers with the weight fraction of PCL of 0.23-0.87, both blocks can crystallize. When the weight fraction of PCL is 0.36 or less, PEO crystallized first. On the contrary, PCL crystallized first when the weight fraction of PCL is 0.43 or more. When the length of the PEG and PCL block is comparable (0.43-0.5), concentric spherulite can be obtained, but the concentric spherulite is not eutectic crystal of PEO and PCL, but originates from step crystallization of PEG and PCL blocks. When the length of the two blocks is quite

different, only spherulite can be observed. The long period of the block copolymer increases gradually as the weight fraction of PCL increasing from 0 to 0.50, due to the increase of the crystalline PCL layer thickness. With further increasing the weight fraction of PCL from 0.50 to 0.87, long period of the copolymer reduced significantly, owing to the depression of the crystalline PEO layer thickness.

Eutectic crystal was observed in symmetric PEG5000-PCL5000 block copolymer-hexanol solution with block molecular weights of ~5000 [42]. Figure 9 shows the AFM micrographs of PEG5000, PCL8000, and PEG5000-PCL5000 single crystals grown from dilute hexanol solution. PEG5000 single crystal is square shaped as shown in Figure 9a, and PCL8000 single crystal is hexagonal shaped as shown in Figure 9(b) [91-93]. PEG5000-PCL5000 single crystal exhibits an elongated hexagonal shape as shown in Figure 9c. The size of PEG5000-PCL5000 single crystals is much larger than those of PEG5000 and PCL5000 single crystals grown under the same conditions. The crystalline structure shown in Figure 9c exhibits coexistence of the two single-crystal layers formed from the two blocks. The PCL blocks crystallize first to form a screw-dislocated lamella with a shape of truncated lozenge, and then the PEG chains fold themselves on the two surfaces of the PCL lamella to achieve a three-layer structure. It is not easy to form eutectic crystals in block copolymers, due to the immiscibility of the unlike blocks. Up to now, eutectic crystals are only observed in symmetric PEG-PCL block copolymers with low molecular weight, and in stereocomplex of polymers blends [94, 95].

Solution grown single crystals of a series of double crystalline diblock

copolymers PLLA-PCL were reported by Casas et al. [96]. Crystalline morphologies depend on the crystallization temperature and the composition. PLLA blocks crystallize firstly, and rendered lozenge, truncated and spindle-shaped crystals can be formed, as shown in Figure 10. The edges of the crystal morphologies are thicker than that in the center, due to PLLA overgrowths in their periphery. An overgrowth of irregular PCL crystals can be also observed during its crystallization. Complex morphologies constituted by lamellar crystals of PCL and PLLA blocks were developed at intermediate temperatures (70 ℃-65 ℃, Figure 10). Electron diffraction patterns (Figure 10) showed the growth of PCL and PLLA crystals.

2.4 Stereocomplexation of enantiomeric block copolymer

Stereocomplexation has been known to take place upon the mixing of two polymers that have the same composition but with different stereo-configurations, e.g. between poly(L/D-2-hydroxybutanoic acid) [94, 95], isotactic/syndiotactic poly(methy methacrylate) (PMMA) [97] and poly(γ-benzyl glutamate) [98-100], PLLA/PDLA [101-106]. The structure of PLLA α-crystal is pseudo-orthorhombic, as shown in Figure 11 (a) [107-111], and the corresponding crystal structure of PDLA is enantiomeric to PLLA crystal. The structure of PLA stereocomplex is shown in Figure 11 (b) and 11 (c) [112]. It shows that the lattice containing a PLLA and a PDLA chain with a 3_1 helical conformation, and they together form an equilateral-triangle-shaped single crystal of PLA stereocomplex. The melting temperature of PLA stereocomplex is 50~60 ℃ higher than that of PLA homopolymer crystal, and the heat-distortion temperature of PLA stereocomplex is

above 100 ℃. Figure 12 shows the thermal properties of PLA stereocomplex of PLLA-PDLA block copolymer (sb-PLA) and of PLLA/PDLA blend (Melt-blend). It can be seen that the melting point of sb-PLA is higher than that of melt-blend, indicating PLLA-PDLA block copolymer enhances the crystallinity and crystal structure of PLA stereocomplex, because the enantiomeric PLLA and PDLA chains are chemically linked and mixed in molecular level. Furthermore, the structure of PLA stereocomplex is related with molecular weight, PLLA/PDLA ratio, and chain architecture [112]. Figure 12 (b) shows the WAXD patterns of PLA homopolymer crystal and PLA stereocomplex crystal. The WAXD pattern of PLA stereocomplex is different from that of PLA homopolymer crystal. In melt-blend, the peak of PLA homopolymer crystal can be observed, due to microscopic phase separation and inhomogeneous distribution of PLLA and PDLA. Generally, only sb-PLA stereocomplex is obtained in symmetric PLLA-PDLA diblock copolymer with the molecular weight of <60 000 g/mol [113]. PLLA-PDLA stereocomplexation may undergo microscopic phase separation in a PDLA-rich and a PLLA-rich phase, which will induce homopolymer crystallization, especially when the molecular weight is high (e. g. 100 000 g/mol) [113-115].

Stereo multiblock poly(lactic acid)s (PLA)s and stereo diblock poly(lactic acid) (DB) with a wide variety of block length of 15.4–61.9 lactyl units are synthesized, and the effects of block length sequence on crystallization and spherulite growth are investigated [116]. Only stereocomplex crystallites are formed in the stereo multiblock PLAs and DB, irrespective of the block length and crystallization

temperature. The melting points the stereo multiblock PLAs and DB increase with increasing block length, but are less than those of PLLA/PDLA blends, as shown in Figure 13. The spherulite growth rates and overall crystallization rates of the stereo multiblock PLAs and DB increased with increasing block length and are lower than that of PLLA/PDLA blend.

Diblock and multiblock PLLA-PDLA copolymers have been synthesized, and the PLLA/PDLA composition can be widely changed. The crystallinity and properties can be controlled by changing the number of blocks, the block length, and the enantiomeric ratio in a chain. In melt crystallization of PLLA-PDLA block copolymer, spherulitic morphology can be observed [113, 114]. Up to now, there are only a few researches on the structure and morphology of PLLA-PDLA block copolymers [106, 106, 115], and should be extensively investigated, because they are close related with the properties and applications.

2.5 Structures of multiblock copolymers

The crystallization and structure of multiblock copolymers become complicated, because of their complicated structure of polymer chains and the confinement from the chemical bonds of the unlike blocks. The architectures of multiblock copolymers can be classified into linear, star-shaped and branched chains. The main application of multiblock copolymers is used as biomaterials, such as shape memory polymers [116-122]. Linear multiblock copolymers comprising of crystallizable poly(butylene succinate) (PBS) hard segments and poly(ethylene glycol) (PEG) (PBS-PEG) soft segments, and poly(ethylene succinate)-b-poly(butylene succinate) (PES-b-PBS)

were synthesized, and the crystallization and structures were investigated [117-119]. The double-crystalline multiblock copolymers formed separated crystalline domains, which determined the permanent shape and temporary shape respectively. The T_m of PEG segment varied with its content ranging from 27.54 to 51.04 ℃, acting as the transition temperature. PBS and PEG segments, PES and PBS segments of the multiblock copolymers are miscible over the entire composition range in the amorphous state. However, PBS, PES and PEG segments in the copolymers can form their own crystals. The crystallization and structure of each segment show strong dependence on its content. Moreover, it is showed that PEG crystalline domains disturb or restrict the crystal growth of PBS lamellae [117]. PBS segment crystallizes firstly, and the PBS crystalline domains confine or affect the crystallization of PES segment. The crystallization of PES segment may break-out and/or is confined within the PBS crystalline domains, and they both determine the final crystalline structure, as shown in Figure 14 [118].

The macromolecular architecture of star-shaped polymers is the unique three-dimensional shaped, and they always exhibit useful properties in comparison with linear polymers, and are expected to display peculiar structures and morphologies. Star-shaped multiblock copolymers of PCL-PLLA [120] and PCL-PEO [121] with different arm number were synthesized and investigated. Star-shaped architecture does not have obvious effect on the crystalline morphologies, though star-shaped polymers have a lower glass-transition temperature, melting temperature, and crystallinity than those of a linear analogue.

As shown in the Figure 15 (A), spherulitic morphologies are observed, indicating 6-armed PCL homopolymer (6sPCL) possesses good crystallizability [120]. The AFM image of 6 armed PCL-PLLA (6sPCL-b-PLLA) multiblock copolymer exhibits tiny morphology (Figure 15 (B)), which should be attributed to the outer PLLA block restricting the crystallization of PCL segment. In all, both the star-shaped architecture and the composition control the crystal growth and morphology.

Crystallization and self-assembly of branched multiblock BBCPs have attracted increasing attention due to the biomedical applications [122]. H-shaped block copolymers of poly(L-lactide)-b-(poly(2-(N,N-dimethylamino) ethyl methacrylate)-b-)poly(ε-caprolactone)(-b-poly(2-(N,N-dimethylamino)ethylmethacrylate))-b-poly(L-lactide) (PLLA-b-(PDMAEMA-b-)PCL(-b-PDMAEMA)-b-PLLA) were synthesized, [123] The crystallinity of PCL and PLLA decreased due to the presence of amorphous PDMAEMA segments in the H-shaped copolymers, as shown in Figure 16. Maltese cross patterns are not found, and the crystalline structure presents flower like morphology for PLLA-B-(N3-)PCL(-N3)-B-PLLA (Figure 16 c). This can be attributed to the decrease of crystallizability of PCL and PLLA segments. PLLA-b-(PDMAEMA-b-)PCL(-b-PDMAEMA)-b-PLLA presented a more complicated spherulitic morphology. The formation of the banded spherulites (as shown in Figure 16 d) is related to lamellar twisting along the radius orientation of the PCL spherulite, which can be attributed to the presence of amorphous PDMAEMA and PLLA crystals. Therefore, the H-shaped copolymer film has better

hydrophilicity than PCL or triblock copolymer of PLLA-b-(N3-)PCL(-N3)-b-PLLA. The unique H-shaped amphiphilic terpolymers, which are composed of biodegradable and biocompatible PCL and PLLA components and intelligent and biocompatible PDMAEMA component, have potential applications in biomedical fields.

2.6 Structures of *BBCP* thin films

Different from bulk materials, microphase separation can also occur in BCP thin films. Except crystallization and microphase separation, the interactions of BCP/substrate interface and air/BCP interface also play an important role in the crystallization behavior and structure formation of BCP thin film. By changing the crystallization pathway, composition, film thickness, and even substrate, the structure of BCP thin film can be regulated. Film thickness is an important factor affecting the structure of block copolymer. In thin films, crystallization and microphase separation are confined. Wetting/dewetting process in thin films may take place, and will affect the structure of the block copolymer by affecting crystallization and micrphase separation [124-126].

Figure 17 shows the crystalline morphologies of PLLA-PEO block copolymer thin films. Hexagonal dendritic morphology which is composed of two sectors arranged alternately, was observed in thin films of 400 nm~200 nm, as shown in Figure 17 a and 17 b [1]. Similar morphology was also observed in PLLA30k-PEO5k block copolymer [17]. In the adjacent two sectors, the chain folding and growth direction were different. In thin film of ~100 nm, lozenge-shaped

lamellae were formed. The stack and the grow crystals are oriented as shown in Figure 17 c. Furthermore, the holes in the center of the lozenge-shaped morphology can be observed, indicating possible de-wetting occur during annealing process. Holes or islands are formed after de-wetting of the thin films, leading to an increase in local polymer chains concentration and orientation of polymer chains at the edge of the holes or islands. Consequently, it becomes easy for the polymer chains to crystallize at the edge of the holes and islands, and then initial crystallization and morphology are observed at the edge of the holes or islands [1, 127-129].

Figure 18 shows the detailed crystalline morphologies of the PLLA16k-b-PEO5k copolymer thin films. Lozenge-spiral dislocation (marked by arrows), lozenge-multilayer was formed in the growth direction. The spacing of lamellae is identical with that of bulk PLLA-PEO, but the size of the lozenge-shaped crystal in thin film is smaller than that of bulk PLLA-PEO. The effect of substrate and 2D confinement of thin film play important role on the peculiar morphology. The morphology of block copolymers in thin film is strongly dependent on the film thickness. Crystallization is severely suppressed due to 2D confinement of thin film, resulting in peculiar structure and morphology [130, 131]. Using a so called micro-evaporation technique, mesoscale dendritic structures were observed in thin films [132-134]. In ultrathin films less than 50 nm, Zhao et al. observed dendritic and fiber-like morphologies of PCL-PEO block copolymer as shown in Figure 19, which is associated with low molecular weight of PCL-PEO block copolymer, and the interaction between microphase separation and crystallization [134].

2.7 Micellar morphology of BBCPs

The self-assembly of block copolymers which contain at least one crystalline block has been another important area of micelle research [135-146]. The understanding of the assembly morphology of amphiphilic block copolymers with a crystalline core structure is still considerably poor, and the improved insight is highly desirable. Nano-sized polymer crystals can acts as seeds for single crystals with regular shape, or for micelles with large size. Block copolymer micelles are generally spherical nano-metric particles or cylindrical nanotube that possess core-shell architecture. They originate from the self-assembly of amphiphilic block copolymers in a selective solvent above a threshold concentration, referred to as the critical aggregation concentration [137].

Monodisperse stereocomplex block copolymer micelles were obtained through the self-assembly of equimolar mixtures of PEG-PLLA-PEG and PEG-PDLA-PEG in water, as shown in Figure 20 [137]. These micelles possessed partially crystallized cores of PLA stereocomplex, and the mean diameter can be regulated by changing PLLA and PDLA content. They exhibited kinetic stability and re-dispersion properties superior to micelles prepared with isotactic or racemic polymers alone. It indicates that stereocomplex has advantages for the formation of stabilized water-soluble nanoparticles.

A hollow strucrure such as nanotubes and vesicles play an important role in biological systems where they provide closed chambers for reation, scaffolding and paking of proteins. Wu et al. synthesized symmetric or asymmetric PEG–PLA–PEG

triblock copolymers. Various architectures such as nanotubes, polymersomes and spherical micelles by self-assemble in aqueous solution were observed, as shown in Figure 21 [138-140]. The changes of morphology and size depended on the chain structure of copolymers.

The self-assembling aggregates of the biodegradable amphiphilic triblock copolymers can be schematically illustrated as Figure 22, (a) spherical polymersomes and (b) cylindrical nanotubes [138-146]. BBCPs consisting of methoxy PEG (mPEG) as a hydrophilic block and either crystalline P(CL-LLA) or amorphous P(CL-DLLA) as a hydrophobic block [141]. Investigations were focused on the effect of the crystalline nature of the core-forming block on the formation of the micelles. Amorphous P(CL-DLLA)-b-mPEG block copolymers adopt a spherical shaped micelles. In contrast, crystalline P(CL-LLA)-b-mPEG block copolymers exhibit a cylindrical shaped micelles. The crystallization of the core-forming blocks of P(CL-LLA) is the driving force for the cylindrical morphology.

Conclusion and Outlook

Biocompatible and biodegradable block copolymers can be miscible, weakly or strongly segregated depending on the compatibility and segregation between the unlike blocks. Competition of crystallization and microphase separation, and/or other driving force can lead to more abundant structures for BBCPs with at least one crystalline block. Some unique structures and morphologies resulting from break-out and confined crystallization, controlled growth of thin film crystallization, eutectic crystal of double crystalline blocks, stereocomplexition of enantiomeric isomers, and

micelles with a crystalline core, can be observed for crystalline-amorphous, crystalline-crystalline diblock, triblock and multiblock copolymers. The assembled structures of the semicrystalline BBCPs can be regulated by changing chemical composition, chain architecture, crystallization pathway, film thickness, and the other internal and external factors.

Structures and morphologies of semicrystalline BBCPs in bulk material have been extensively studied and well understood in diblock, triblock and multiblock copolymers. Researches on the relationship among the chemical composition, macromolecular architectures, thermal history, physical properties, mechanical performance, biodegradability and biocompatibility of BBCPs are frequently neglected. Meanwhile, the controlled nano-scale structures, the orientation of lamellar crystals, the relationship between structure and function of BBCPs, crystallization kinetics in ultra-thin films, confined crystallization from crystal lamellae and glass state should be more and further studied. Extensive studies are need for nano-structures and microscopic morphology of stereocomplex, including PLLA-PDLA, PLLA-PD2HB, PDLA-PL2HB diblock and multi-block copolymers. Controlled growth and micro-structure, growth kinetics of semicrystalline micelles of BBCPs are of importance for applications in biomedical area, and should be extensively studied.

Acknowledgements

This work is financially supported by the National Natural Science Foundation of China (21374077, 51173130 and 51103151).

Conflicts of interest

The authors declare no conflict of interest.

References

1. Huang, S. Y.; Jiang, S. C.; Chen, X. S.; An, L. J. Dendritic Superstructures and Structure Transitions of Asymmetric Poly(L-lactide-b-ethylene oxide) Diblock Copolymer Thin Films, *Langmuir*, **2009**, *25 (22)*, 13125-13132.
2. Nair, L. S.; Laurencin, C. T. Biodegradable polymers as biomaterials, *Prog Polym Sci*, **2007**, *32*, 762-798.
3. Castillo, R. V.; Müller, A. J. Crystallization and morphology of biodegradable or biostable single and double crystalline block copolymers, *Prog Polym Sci*, **2009**, *34*, 516-560.
4. Kumar, N.; Ravikumar, M.; Domb, A.; Biodegradable block copolymers. *Adv Drug Deliv Rev* **2001**, *53*, 23-44.
5. Kissel, T.; Li, Y.; Unger, F. ABA-triblock copolymers from biodegradable polyester A blocks and hydrophilic poly(ethylene oxide) B-blocks as a candidate for in situ forming hydrogel delivery system for proteins. *Adv Drug Deliv Rev* **2002**, *54*, 99-134.
6. Harada, A.; Kataoka, K.; Supra-molecular assemblies of block copolymers in aqueous media as nanocotainers relevant to biological applications. *Prog Polym Sci* **2006**, *31*, 949-982.
7. Kim, J. H.; Park, K.; Nam, H. Y.; Lee, S.; Kim, K.; Kwon, I. C. Polymers for bioimaging. *Prog Polym Sci* **2007**, *32*, 1031-1053.

8. Martina, M.; Hutmacher, D. W. Biodegradable polymers applied in tissue engineering research: a review. *Polym Int* **2007**, *56*, 145-157.

9. Rzaev, Z.; Dinçer, S.; Piskin, E. Functional copolymers of N-isopropylacrylamide for bioengineering applications. *Prog Polym Sci* **2007**, *32*, 534-595.

10. Rapoport, N. Physical stimuli-responsive polymeric micelles for anti-cancer drug delivery. *Prog Polym Sci* **2007**, *32*, 962-990.

11. Discher, D.; Ortiz, V.; Srinvas, G.; Klein, M.; Kim, Y. Christian, D. Emerging applications of polymersomes in delivery: from molecular dynamics to shringkage of tumors, *Prog Polym Sci* **2007**, *32*, 838-857.

12. Hamley, I. W. Crystallization in block copolymer, *Adv Polym Sci* **1999**, *148*, 113-137.

13. Müller, A. J.; Balsamo, V.; Arnal, M. L. Nucleation and crystallization in diblock and triblock copolymers, *Adv Polym Sci* **2005**, *190*, 1-63.

14. Jiang, S. C.; He, C.; An, L. J.; Chen, X.; Jiang, B. Z. Crystallization and ring-banded spherulite morphology of poly(ethylene oxide)-block-poly(ε-caprolactone) diblock copolymer. *Macromol Chem Phys* **2004**, *205*, 2229-2234.

15. Rashkov, I.; Manolova, N.; Li, S. M.; Espartero, J. L.; Vert, M. Synthesis, characterization, and hydrolytic degradation of PLA/PEO/PLA triblock copolymers with short poly(L-lactic acid) chains. *Macromolecules* **1996**, *29*, 50-56.

16. Mothé, C. G.; Drumond, W. S.; Wang, S. H. Phase behavior of biodegradable amphiphilic poly(L-lactide)-b-poly(ethylene glycol)-b-poly(L-lactide). *Thermochim Acta* **2006**, *445*, 61-66.

17. Huang, S. Y.; Jiang, S. C.; Chen, X.; An, L. J. Crystallization and Morphology of Poly(ethylene oxide-b-lactide) Crystalline-Crystalline Diblock Copolymers *J. Poly. Sci. Part B: Poly. Phys.* **2008**, 46, 1400-1411.

18. Sun, J.; Hong, Z.; Yang, L.; Tang, Z.; Chen, X.; Jing, X. Study on crystalline morphology of poly(L-lactide)-poly(ethylene glycol) diblock copolymer. *Polymer* **2004**, *45*, 5969-5977.

19. Hamley, I. W.; The physics of block copolymers. Oxford, Oxford University Press, **1998**.

20. Hadjichistidis, N.; Pispas, S. Floudas, G. Block copolymers: synthetic strategies, physical properties and applications. New Jersey, Wiley, **2003**.

21. He, W. N.; Xu, J. T. Crystallization assisted self-assembly of semicrystalline block copolymers, *Prog Polym Sci* **2012**, *37*, 1350-1400.

22. Bates, F. S.; Fredrickson, G. H. Block copolymers: designer soft materials. *Phys Today* **1999**, *52*, 32-38.

23. Kim, J. K.; Yang, S. Y.; Lee, Y.; Kim, Y. Functional nanomaterials based on block copolymer self-assembly. *Prog Polym Sci 2011*, *35*, 1325–1349.

24. Loo, Y. L.; Register, R. A.; Ryan, A. J. Polymer crystallization in 25 nm spheres. *Phys Rev Lett* **2000**, *84*, 4120-4123.

25. Tirumala, V. R.; Romang, A.; Agarwal, S.; Lin, E. K.; Watkins J. J. Well Ordered

Polymer Melts from Blends of Disordered Triblock Copolymer Surfactants and Functional Homopolymers. *Adv. Mater.* **2008**, *9999*, 1-6.

26. Zhu, L.; Cheng, S. Z. D.; Huang, P.; Ge, Q.; Quirk, R. P.; Thomas, E. L.; Lotz, B.; Hsiao, B. S.; Yeh, F.; Liu L. Nanoconfined Polymer crystallization in the hexagonally perforated layers of a self-assembled PS-b-PEO diblock copolymer. *Adv. Mater.* **2002**, *14*, 31-34.
27. Lee, J.; Bae, Y. H.; Sohn, Y. S.; Jeong, B. Thermogelling aqueous solutions of alternating multiblock copolymers of poly(L-lactic acid) and poly(ethylene glycol). *Biomacromolecules* **2006**, *7*, 1729-1734.
28. Zhang, J.; Wang, L. Q.; Wang, H.; Tu, K. Micellization phenomena of amphiphilic block copolymers based on methoxy poly(ethylene glycol) and either crystalline or amorphous poly(caprolactone-b-lactide). *Biomacromolecules* **2006**, *7*, 2492-2500.
29. Fu, J.; Luan, B.; Yu, X.; Cong, Y.; Li, J.; Pan, CY.; Han, YC.; Yang, YM.; Li, BY. Self-assembly of crystalline coil diblock copolymer in solvents with varying selectivity: from spinodal-like aggregates to spheres, cylinders, and lamellae. *Macromolecules* **2004**, *37*, 976 986
30. Harada, A.; Kataoka, K. Supramolecular assemblies of block copolymers in aqueous media as nanocontainers relevant to biological applications. *Prog Polym Sci* **2006**, *31*, 949–982.
31. Li, Q.; He, J.; Glogowski, E.; Li, X.; Wang, J.; Emrick, T.; Russell, TO. Responsive Assemblies: Gold Nanoparticles with Mixed Ligands in Microphase

Separated Block Copolymers. Adv. Mater. 2008, 9999, 1–5

32. Kim, J.; Park, K.; Nam, HY; Lee, S; Kim, K.; Kwon, IC. Polymers for bioimaging. *Prog Polym Sci* **2007**, *32*, 1031–1053.
33. Rzaev, ZMO.; Dinçer, S.; Piskin, E. Functional copolymers of N-isopropylacrylamide for bioengineering applications. *Prog Polym Sci* **2007**, *32*, 534–595.
34. Jeong, U.; Kim, H.; Rodriguez, R. L.; Tsai, I. Y.; Stafford, C. M.; Kim, J.; Hawker, C. J.; Russell, T. P. Asymmetric Block Copolymers with Homopolymers: Routes to Multiple Length Scale Nanostructures, *Adv. Mater.* **2002**, *14*, 274-276.
35. Rangarajan, P.; Register, R. A.; Adamson, D, H.; Fetters, L. J.; Bras, W.; Naylor, S.; Ryan, A. J. Dynamics of structure formation in crystallizable block copolymers. *Macromolecules* **1995**, *28*, 1422–1428.
36. Ryan, A. J.; Hamley, I.W.; Bras, W.; Bates, F. S. Structure development semicrystalline diblock copolymers crystallizing from the ordered melt. *Macromolecules* **1995**, *28*, 3860–3868.
37. Nojima, S.; Akutsu, Y.; Washino, A.; Tanimoto, S.; Morphology of melt-quenched poly(epsilon-caprolactone)-block-polyethylene copolymers. Polymer **2004**, 45, 7317–24.
38. Lipik, V.T.; Kong, J.F.; Chattopadhyay, S.; Widjaja, L.; Liow, S. S.; Venkatraman. S.S.; Abadie, M. J.M. Thermoplastic biodegradable elastomers based on e-caprolactone and L-lactide block co-polymers: A new synthetic

approach. *Acta Biomaterialia* **2010**, *6*, 4261–4270.

39. Hamley, I. W.; Castelletto, V.; Castillo, R. V.; Müller, A. J.; Martin, C. M. Crystallization in poly(l-lactide)-b-poly(epsilon- caprolactone) double crystalline diblock copolymers: a study usingX-ray scattering, differential scanning calorimetry, and polarized optical microscopy. Macromolecules **2005**, 38, 463–472.
40. He, C.; Sun, J.; Zhao, T.; Hong, Z.; Chen, X. Formation of a unique crystal morphology for the poly(ethylene glycol)-poly(ε-caprolactone) diblock copolymer. *Biomacromolecules* **2006**, *7*, 252-258.
41. He, C.; Sun, J.; Ma, J.; Chen, X.; Jing, X. Composition dependence of the crystallization behavior and morphology of the poly(ethylene glycol)-poly(ε-caprolactone) diblock copolymer. *Biomacromolecules* **2006**, *7*, 3482-3489.
42. Sun, J.; Chen, X.; He, C.; Jing, X. Morphology and structure of single crystals of poly(ethylene glycol)-poly(ε-caprolactone) diblock copolymers. *Macromolecules* **2006**, *39*, 3717-3719.
43. Nojima, S.; Kato, K.; Yamamto, S.; Ashida, T. Crystallization of block copolymers. 1. Small angle X-ray scattering study of an epsilon-caprolactone butadiene diblock copolymer. *Macromolecules* **1992**, *25*, 2237-2242.
44. Ryan, A.; Hamley, I.; Bras, W.; Bates, F. Strcuture development in semicrystalline diblock copolymers crystallizing from the ordered melt. *Macromolecules* **1995**, *28*, 3860-3868.

45. Rangrajan, P.; Register, R.; Fetters, L.; Bras, W.; Naylor, S.; Ryan, A. Crystallization of a weakly segregated polyolefin diblock copolymer. *Macromolecules* **1995**, *28*, 4932-4938.

46. Floudas, G.; Ulrich, R., Wiesner, U. Microphase separation in poly(isoprene-b-ethylene oxide) diblock copolymer melts. 1. Phase state and kinetics of the order-to-order transition. *J Chem Phys* **1999**, *110*, 652-663.

47. Li, S.; Rashkov, I.; Espartero, J.; Manolova, N.; Vert, M. Synthesis, characterization, and hydrolytic degradation of PLA/PEO/PLA triblock copolymers with long poly(L-lactic acid) blocks. *Macromolecules*, **1996**, *29*, 57-62.

48. Kim, K.; Chung, S.; Chin, I.; Kim, M.; Yoon, J. Crystallization behavior of biodegradable amphiphilic poly(ethylene glycol)-poly(L-lactide) block copolymers. *J Appl Polym Sci* **1999**, *72*, 341-348.

49. Kubies, D.; Rypácek, F.; Kovárová, J.; Lednický, F. Micro-domain structure in polylactide-block-poly(ethylene oxide) copolymer films. *Biomaterials* **2000**, *21*, 529–536.

50. Maglio, G.; Migliozzi, A.; Palumbo, R. Thermal properties of di- and triblock copolymers of poly(l-lactide) with poly(oxyethylene) or poly(e-caprolactone). *Polymer* **2003**, *44*, 369–375.

51. Cai, C.; Wang, L.; Dong, C. M. Synthesis, characterization, effect of architecture on crystallization, and spherulitic growth of poly(L-lactide)-b-poly(ethylene oxide) copolymers with different branch arms. *J Polym Sci Part A Polym Chem*

2006, *44*, 2034–2244.

52. Huang, C. I.; Tsai, S. H.; Chen, C. M. Isothermal crystallization behavior of poly(l-lactide) in poly(l-lactide)-block-poly(ethylene glycol) diblock copolymers. *J Polym Sci Part B Polym Phys* **2006**, *44*, 2438–2448.
53. Wu, T.; He, Y.; Fan, Z.; Wei, J.; Li, S. Investigations on themorphology and melt crystallization of poly(L-lactide)-poly(ethylene glycol) diblock copolymers. *Polym Eng Sci* **2008**, *48*, 425–433.
54. Huang, S. Y.; Li, H, F.; Jiang, S. C.; Chen, X. S.; An, L. J. Morphologies and structures in poly(L-lactide-b-ethylene oxide) copolymers determined by crystallization, microphase separation, and vitrification. *Polym Bull* **2011**, *67*, 885–902.
55. Gan, Z.; Jiang, B.; Zhang, J. Poly(ε-caprolactone)/poly(ethylene oxide) diblock copolymer. I: Isothermal crystallization and melting behavior. *J Appl Polym Sci* **1996**, *59*, 961–967.
56. Gan, Z.; Zhang, J.; Jiang B. Poly(ε-caprolactone)/poly(ethylene oxide) diblock copolymer. II: Nonisothermal crystallization and melting behavior. *J Appl Polym Sci* **1997**, *63*, 1793–1804.
57. Choi, Y. K.; Bae, Y. H.; Kim, S. W. Star-shaped poly(ether-ester) block copolymers: synthesis, characterization, and their physical properties. *Macromolecules* **1998**, *31*, 8766–8774.
58. Bogdanov, B.; Vidts, A.; Schacht, E.; Berghmans, H. Isothermal crystallization of poly(ε-caprolactone-ethylene glycol) block copolymers. *Macromolecules*

1999, *32*, 726–731.

59. Lu, C.; Guo, S. R.; Zhang, Y.; Yin, M. Synthesis and aggregation behavior of four types of different shaped PCL-PEG block copolymers. *Polym Int* **2006**, *55*, 694–700.

60. Takeshita, H.; Fukumoto, K.; Ohnishi, T.; Ohkubo, T.; Miya, M.; Takenaka, K. Formation of lamellar structure by competition in crystallization of both components for crystalline–crystalline block copolymers. *Polymer* **2006**, *47*, 8210–8218.

61. Li, L.; Meng, F.; Zhong, Z.; Byelov, D.; de Jeu, W. H.; Feijen, J. Morphology of a highly asymmetric double crystallizable poly(ε-caprolactone-b-ethylene oxide) block copolymer. *J Chem Phys* **2007**, *126*, 024904.

62. Castillo, R. V.; Müller, A. J.; Raquez, J. M.; Dubois, P. Crystallization Kinetics and Morphology of Biodegradable Double Crystalline PLLA-b-PCL Diblock Copolymers. *Macromolecules* **2010**, *43*, 4149-4160.

63. Ho, R. M.; Hsieh, P.; Tseng, W.; Lin, C.; Huang, B.; Lotz, B. Crystallization-induced orientation for microstructures of poly(L-lactide)-b-poly(ε-caprolactone) diblock copolymers. *Macromolecules* **2003**, *36*, 9085–9092.

64. Hamley, I.; Parras, P.; Castelletto, V.; Castillo, R.; Müller, A. J.; Pollet, E. et al. Melt structure and its transformation by sequential crystallization of the two blocks within poly(L-lactide)-block-Poly(ε-caprolactone) double crystalline diblock copolymers. *Macromol Chem Phys* **2006**, *207*, 941–953.

65. Bogdanov, B.; Vidts, A.; Van Den Bulcke, A.; Verbeeck, R.; Schacht, E. Synthesis and thermal properties of poly(ethylene glycol)-poly(-caprolactone) copolymers. *Polymer* **1998**, *39*, 1631-1636.

66. Piao, L.; Dai, Z.; Deng, M.; Chen, X.; Jing, X. Synthesis and characterization of PCL/PEG/PCL triblock copolymers by using calcium catalyst. *Polymer* **2003**, *44*, 2025-2031.

67. Ghoroghchian, P.; Li, G.; Levine, D.; Davis, K.; Bates, F.; Hamer, D.; et al. Bioresorbable vesicles formed through spontaneous self-assembly of amphiphilic poly(ethylene oxide)-block-polycaprolactone. *Macromolecules* **2006**, *39*, 1673-1675.

68. Loo, Y. L.; Register, R. A.; Ryan, A. J.; Dee, G. T. Polymer crystallization confined in one, two, or three dimensions. *Macromolecules* **2001**, *34*, 8968-8977.

69. Yang, J.; Zhao, T.; Zhou, Y.; Liu, L.; Li, G.; Zhou, E.; Chen, X. Single Crystals of the Poly(L-lactide) Block and the Poly(ethylene glycol) Block in Poly(L-lactide) poly(ethylene glycol) Diblock Copolymer. *Macromolecules* **2007**, *40*, 2791-2797.

70. Yang, J.; Liang, Y.; Luo, J.; Zhao, C.; Han, Charles C. Multilength Scale Studies of the Confined Crystallization in Poly(L-lactide)-block-Poly(ethylene glycol) Copolymer. *Macromolecules* **2012**, *45*, 4254−4261.

71. Kikkawa, Y.; Abe, H.; Iwata, T.; Inoue, Y.; Doi, Y. Crystallization, stability, and enzymatic degradation of poly(L-lactide) thin film. *Biomacromolecules*, **2002**, *3*,

350-356.

72. Nurkhamidah, S.; Woo, E. M. Phase-Separation-Induced Single-Crystal Morphology in Poly(L-lactic acid) Blended with Poly(1,4-butylene adipate) at Specific Composition. *J. Phys. Chem. B* **2011**, *115*, 13127–13138.

73. Hamley, I. W. The physics of block copolymers. Oxford, Oxford university press. 1998.

74. Kim, J.; Park, D.; Lee, M. Ihn, K. Synthesis and crystallization behavior of poly(L-lactide)-block-poly(ε-caprolactone) copolymer. Polymer **2001**, *42*, 7429-7441.

75. Zhu, L.; Calhoun, B. H.; Ge, Q.; Quirk, R. P.; Cheng, SZD. Thomas, E. L.; et al. Initial-stage growth controlled crystal orientation in nanoconfined lamellae of a sell-assembled ceystalline-amorphous diblock copolymer. *Macromolecules* **2001**, *34*, 1244-1251.

76. Ho, RM.; Hsieh, PY.; Tseng, WH.; Lin, CC.; Huang, BH.; Lotz, B. Crystallization-induced orientation for microstructure of poly(L-lactide)-b-poly(ε-caprolactone) diblock copolymers. *Macromolecules* **2003**, *36*, 9085-9092.

77. De Rosa, C.; Park, C.; Lotz, B.; Wittmann, J.; Fetters, L.; Thomas, E.; Control of molecular and microdomain orientation in a semicrystalline block copolymer thin film by epitaxy. *Macromolecules* **2000**, *33*, 4871-4876.

78. Park, C.; De Rosa, C.; Thomas, E. Large area orientation of block copolymer microdomains in thin films via directional crystallization of a solvent.

Macromolecules **2001**, *34*, 2602-2606.

79. Kikkawa, Y.; Abe, H.; Iwata, T.; Inoue, Y.; Doi, Y. In situ observation of crystal growth for poly[(S)-lactide] by temperature-controlled atomic force microscopy. *Biomacromolecules* **2001**, *2*, 940-945.
80. Liu, L.; Jiang B. Z.; Zhou, E. L. Study of semicrystalline-amorphous diblock copolymers. 1. Microphase separation, glass transition and crystallization of tetrahydrofuran methyl methacrylate diblock copolymers. *Polymer* **1996**, *37*, 3937–43.
81. Quiram, D.; Register, R.; Marchand, G. Crystallization of asymmetric diblock copolymers from microphase-separated melts. *Macromolecules* **1997**, *30*, 4551–4558.
82. Quiram, D.; Register, R.; Marchand, G.; Ryan, A. Dynamics of structure formation and crystallization in asymmetric diblock copolymers. *Macromolecules* **1997**, *30*, 8338–8343.
83. Hamley, I. W.; Fairclough, J.; Bates, F.; Ryan, A. Crystallization thermodynamics and kinetics in semicrystalline diblock copolymers. *Polymer* **1998**, *39*, 1429–1437.
84. Shiomi, T; Tsukada, H; Takeshita, H.; Takenaka, K.; Tezuka, Y. Crystallization of semicrystalline block copolymers containing a glassy amorphous component. *Polymer* **2001**, *42*, 4997–5004.
85. Nojima, S.; Hashizume K.; Rohadi, A.; Sasaki S. Crystallization of epsilon-caprolactone blocks within a crosslinked microdomain structure of

poly(epsilon-caprolactone)-block-polybutadiene. *Polymer* **1997**, *38*, 2711–2718.

86. Kelarakis, A.; Mai, S. M.; Booth, C.; Ryan, A. J.; Can rheometry measure crystallization kinetics: A comparative study using block copolymers. *Polymer* **2005**, *46*, 2739–47.

87. Nojima, S.; Inokawa, D.; Kawamura, T.; Nitta, K. Dynamic mechanical study of block copolymer crystallization confined within spherical nanodomains. *Polym J* **2008**, *40*, 986–991.

88. Xu, J.; Bellas, V.; Jungnickel, B.; Stuhn, B.; Rehahn, M. Equilibrium melting temperature of poly(ferrocenyl dimethylsilane) in homopolymers and lamellar diblock copolymers with polystyrene. *Macromol Chem Phys* **2010**, 211, 1261–1271.

89. Xue, F. F.; Chen, X. S.; An, L. J.; Funari, S. S.; Jiang, S. C. Soft nanoconfinement effects on the crystallization behavior of asymmetric poly(ethylene oxide)-block-poly(ε-caprolactone) diblock copolymers. *Polym Int* **2012**, *61*, 909–917.

90. Jiang, S. C.; He. C. L.; Men, Y. F.; Chen, X.; An, L. J.; Funari, S. S.; Chan, C. M. Study of temperature dependence of crystallisation transitions of a symmetric PEO-PCL diblock copolymer using simultaneous SAXS and WAXS measurements with synchrotron radiation. *Eur. Phys. J. E* **2008**, *27*, 357–364.

91. Núñez, E.; Gedde, U.W. Single crystal morphology of star-branched polyesters with crystallisable poly(ε-caprolactone) arms. *Polymer* **2005**, *46,* 5992-6000.

92. Mareau, V. H.; Prud'homme, R. E. In-situ hot stage atomic force microscopy

study of poly(ε-caprolactone) crystal growth in ultrathin films. *Macromolecules* **2005**, *38*, 398-408.

93. Tsuji, H.; Hosokawa, M.; Sakamoto, Y. Ternary stereocomplex formation of one L-configured and two D-configured optically active polyesters, poly(L-2-hydroxybutanoic acid), poly(D-2-hydroxybutanoic acid), and poly(D-lactic acid). *ACS Macro Let.* **2012**, *1*, 687−691.
94. Tsuji, H.; Nakano, M.; Hashimoto, M.; Takashima, K.; Katsura, S.; Mizuno A. Electrospinning of Poly(lactic acid) Stereocomplex Nanofibers. *Biomacromolecules* **2006**, *7*, 3316-3320
95. Watanabe, W.H., Ryan, C.F., Fleischer, Jr, P.C., Garrett, B.S. Measurement of the tacticity of syndiotactic poly-(methyl methacrylate) by the gel melting point. *J Phys Chem* **1961**, *65*, 896.
96. Casas, M.T.; Puiggali, J.; Raquez, J.M.; Dubois, P.; Córdova, M.E.; Müller, A. J. Single crystals morphology of biodegradable double crystalline PLLA-b-PCL diblock copolymers. Polymer 2011, 52, 5166-5177.
97. Fukuzawa, T., Uematsu, I., Uematsu, Y. Physical properties of mixtures of poly(γ -benzyl-L-glutamate) and poly(γ -benzyl-D-glutamte). *Polym J* **1974**, *6*, 537–541.
98. Matawhima, N., Hikichi, K., Tsutsumi, A., Kaneko, M. X-ray scattering of synthetic poly(α-amino acid)s in the solid state. II. Phase transition ofDLmixtures of poly(γ -benzyl glutamate)s. *Polym J* **1975**, *3*, 382–386.
99. Baba, Y., Kagemoto, A. Heats of dissociation of mixture of poly(γ -benzyl L-

and D-glutamate). *Macromolecules* **1977**, *10*, 458–460.

100. Ikada, Y., Jamshidi, K., Tsuji, H., Hyon, S.-H. Stereocomplex formation between enantiomeric poly(lactides), *Macromolecules* **1987**, *20*, 904–906.

101. Yui, N., Dijkstra, P. J., Feijen, J. Stereo block copolymers of L-and D-lactides. *Makromol. Chem.* **1990**, *191*, 481–488.

102. Spassky, N.,Wisniewski,M., Pluta, C., Le Borgne, A. Highly stereoelective polymerization of rac-(D,L)-lactide with a chiral Schiff's base/aluminium alkoxide initiator. *Macromol Chem Phys* **1996**, *197*, 2627–2637.

103. Fukushima, K: Furuhashi, Y., Sogo, K., Miura, S., Kimura, Y. Stereoblock poly(lactic acid):synthesis via solid-state polycondensation of a stereocomplexed mixture of poly(L-lactic acid) and poly(D-lactic acid). *Macromol. Biosci.* **2005**, *5*, 21–29.

104. Fukushima, K., Hirata, M.; Kimura, Y. Synthesis and characterization of stereoblock poly(lactic acid)s with nonequivalent D/L sequence ratios. *Macromolecules* **2007**, *40*, 3049–3055

105. Hirata, M., Kimura, Y., Thermomechanical properties of stereoblock poly(lactic acid)s with different PLLA/PDLA block compositions. *Polymer* **2008**, *49(11)*, 2656–2661.

106. Kakuta, M.; Hirata, M.; Kimura, Y. Stereoblock Polylactides as High-Performance Bio-Based Polymers. *J Macromolecular Sci R, Part C: Polymer Reviews* **2009**, *49*, 107–140.

107. De Santis, P., Kovacs, A.J. Molecular conformation of poly(S-lactic acid).

Biopolymers **1968**, *6*, 299–306.

108. Hoogsten, W., Postema, A.R., Pennings, A.J., ten Brinke, G., Zugenmair, P. Crystal structure, conformation, and morphology of solution-spun poly(L-lactide) fibers. *Macromolecules* **1990**, *23*, 634–642.

109. Kobayashi, J., Asahi, T., Ichiki, M., Oikawa, A., Suzuki, H., Watanabe, T., Fukada, E., Shikinami, Y. "Structural and optical properties of poly lactic acids", J. Appl. Phys. **1995**, 77, 2957–2973.

110. Miyata, T.,Masuko, T. Morphology of poly(L-lactide) solution-grown crystals. *Polymer* **1997**, *38*, 4003–4009.

111. Okihara, T., Tsuji,M., Kawaguchi, A., Katayama, K., Tsuji, H., Hyon, S.-H., Ikada, Y. Crystal structure of stereocomplex of poly(L-lactide) and poly(D-lactide). *J. Macromol. Sci., Phys.***1991**, *B30*, 119–140.

112. Tsuji, H., Ikada, Y. Stereocomplex formation between enantiomeric poly(lactic acid)s. Stereocomplexation from the melt, *Macromolecules* **1993**, *26*, 6918–6926

113. Tsuji, H. Poly(lactide) Stereocomplexes: Formation, Structure, Properties, Degradation, and Applications. *Macromol. Biosci.* **2005**, *5*, 569–597

114. Rahaman, M. H.; Tsuji, H. Isothermal Crystallization and Spherulite Growth Behavior of StereoMultiblock Poly(lactic acid)s: Effects of Block Length. *J. Appl. Polym. Sci.* **2013**, *129*, 2502-2517.

115. Uehara, H.; Karaki, Y.; Wada, S.; Yamanobe, T. Stereo-complex crystallization of poly(lactic acid)s in block-copolymer phase separation. *ACS Applied*

Materials Interfaces **2010**, *2 (10)*, 2707-2710.

116. Rahaman, Md. H.; Tsuji, H. Isothermal crystallization and spherulite growth behavior of stereo multiblock poly(lactic acid)s: effects of block length. *J. Appl. Polym. Sci.* **2013**, *129*, 2502–2517.

117. Huang, CL.; Jiang, L.; Zhang, J.; Zeng, J.; Yang, K.; Wang, Y. Z. Poly(butylene succinate)-poly(ethylene glycol) multiblock copolymer: Synthesis, structure, properties and shape memory performance. *Polymer Chemistry* **2012**, *3*, 800-808.

118. Zeng, J.; Zhu, Q.; Lu, X.; He, Y.; Wang, Y. Z. From miscible to partially miscible biodegradable double crystalline poly(ethylene succinate)-b-poly(butylene succinate) multiblock copolymers. Polym. Chem., **2012**, *3*, 399–408.

119. Huang, C.L.; Jiao, L.; Zeng, J.B.; Zhang, M.; Xiao, L.P.; Yang, K.K.; Wang, Y.Z. Crystallization behavior and morphology of double crystalline poly (butylene succinate)-poly(ethylene glycol) multiblock copolymers. Polymer 2012, 53, 3780-3790.

120. Zhang, Z.; Ren, J.; Feng, Y.; Li, J.; Yuan, W. Z. Microwave-Assisted Synthesis of Star-Shaped Poly(e-caprolactone)-block-poly(L-lactide) Copolymers and the Crystalline Morphologies. *Journal of Polymer Science: Part A: Polymer Chemistry* **2010**, *48*, 5063–5071.

121. Dong, C. M.; Qiu, K. Y.; Gu, Z. W.; Feng, X. D. Poly(ε-caprolactone)-b-(D,L-lactic acid-alt-glycolic acid) with Multifunctional

Initiator and SnOct2 Catalys. *Macromolecules* **2001**, *21*, 4691–4696;

122. Jin, H.; Huang, W.; Zhu, X.; Zhou, Y. F.; Yan, D. Y. Biocompatible or biodegradable hyperbranched polymers: from self-assembly to cytomimetic applications. *Chem Soc Rev* **2012**, *41*, 5986-5997.

123. Yuan, W. Z.; Zhang, J.; Zou, H.; Ren, J. Synthesis, crystalline morphologies, self-assembly, and properties of H-shaped amphiphilic dually responsive terpolymers. *J Polym Sci Part A: Polym Chem* **2012**, *50*, 2541–2552.

124. Hamley, I. W. Ordering in thin films of block copolymers: fundamentals to potential applications. *Prog Polym Sci* **2009**, *34*, 1161–210.

125. Segalman, R. A.; Patterning with block copolymer thin films. *Mater Sci Eng R* **2005**, *48*, 191–226.

126. Ramanathan, M.; Darling, S. B. Mesoscale morphologies in polymer thin films. *Prog Polym Sci* **2011**, *36*, 793–812.

127. Zhang, F. J.; Chen, Y. Z.; Huang, H. Y.; Hu, Z. J.; He, T. B. Boundary effect of relief structure on crystallization of diblock copolymer in thin films. *Langmuir* **2003**, *19*, 5563–6.

128. Zhang, F. J.; Huang, H. Y.; Hu, Z. J.; Chen, Y. Z.; He, T. B. Crystallization of weakly segregated poly(styrene-b-epsilon-caprolactone) diblock copolymer in thin films. *Langmuir* **2003**, *19*, 10100–8.

129. Fu, J.; Cong, Y.; Li, J.; Luan, B.; Pan, C. Y.; Yang, Y. M.; Li, B. Y.; Han, Y. Hole nucleation and growth induced by crystallization and microphase separation of thin semicrystalline diblock copolymer films. *Macromolecules* **2004**, *37*,

6918–25.

130. Li, Y.; Loo, Y. L.; Register, R. A.; Green, P. F. Influence of interfacial constraints on the morphology of asymmetric crystalline-amorphous diblock copolymer films. *Macromolecules* **2005**, *38*, 7745–7753.

131. Huang, W. H.; Luo, C. X.; Zhang, J. L.; Han, Y. C. Formation of ordered microphase-separated pattern during spin coating of ABC triblock copolymer. *J Chem Phys* 2007, 126, 104901/1-9.

132. Huang, S. Y.; Li, HF.; Shang, YR.; Yu, DH.; Li, G.; Jiang, SC.; Chen, XS.; An, LJ. Chloroform micro-evaporation induced ordered structures of poly(L-lactide) thin films. *RSC Advances* **2013**, *3*, 13705–13711

133. Huang, S. Y.; Li, HF.; Wen, HY.; Yu, DH.; Jiang, SC.; Li, G.; Chen, XS.; An, LJ. Solvent micro-evaporation and concentration gradient synergistically induced crystallization of poly(L-lactide) and ring banded supra-structures with radial periodic variation of thickness. *CrystEngComm* **2014**, *16*, 94–101.

134. Zhao, J. C.; Zhang, J. M.; Duan, X. L.; Peng, Z.; Wang, S. H. Formation mechanism, chain folding, and growth behavior of the intriguing fiber-like crystal of poly (ethylene oxide-b-epsilon-caprolactone) block copolymer in ultrathin films. *Polymer* **2011**, *52*, 2085–93.

135. Vilgis, T.; Halperin, A. Aggregation of coil crystalline block copolymers-equilibrium crystallization. *Macromolecules* **1991**, *24*, 2090-2095.

136. Cao, L.; Manners, I.; Winnik, M. A. Influence of the interplay of crystallization and chain stretching on micellar morphologies solution self-assembly of

coil-crystalline poly(isoprene-block ferrocenylsilane). *Macromolecules* **2002**, *35*, 8258-8260.

137. Kang, N.; Perron, MÉ.; Prud'homme, R. E.; Zhang, Y. B.; Gaucher, G.; Leroux, G. C. Stereocomplex Block Copolymer Micelles: Core−Shell Nanostructures with Enhanced Stability. *Nano Lett* **2005**, *5 (2)*, 315-319.

138. Spasova, M.; Manolova, N.; Paneva, D.; Mincheva, R. Dubois, P.; Rashkov, I.; Maximova, V.; Danchev, D. Polylactide Stereocomplex-Based Electrospun Materials Possessing Surface with Antibacterial and Hemostatic Properties. *Biomacromolecules* **2010**, *11*, 151–159.

139. Huitron-Rattinger, E.; Ishida, K.; Romo-Uribe, A.; Mather, P. T. Thermally modulated nanostructure of poly(ε-caprolactone)Eposs multiblock thermoplastic polyurethane. *Polymer* **2013**, *54*, 3350-3362.

140. Wu, X. H.; Li, S.; Coumes, F.; Darcos, V.; Him, J. L. K.; Bron, P. Modeling and self-assembly behavior of PEG–PLA–PEG triblock copolymers in aqueous solution. *Nanoscale* **2013**, *5*, 9010–9017.

141. Zhang, J.; Wang, L. Q.; Wang, H. J.; Tu, K. H. Micellization phenomena of aphiphilic block copolymers based on methoxy poly(ethylene glycol) and either crystallineor amorphous poly(caprolactone-b-lactide). *Biomacromolecules* **2006**, *7*, 2492-2500.

142. Payyappilly, S.; Dhara, S.; Chattopadhyay, S. Thermoresponsive biodegradable PEG-PCL-PEG based injectable hydrogel for pulsatile insulin delivery. *J Biomed Mater Res Part A* **2014**, *102A*, 1500–1509.

143. Wang, H.; He, J.; Zhang, M.Z.; Tao, Y.F.; Li, F.; Tamb, K.C.; Ni, P. H. Biocompatible and acid-cleavable poly(ε-caprolactone)-acetal-poly(ethylene glycol)-acetal-poly(ε-caprolactone) triblock copolymers: synthesis, characterization and pH-triggered doxorubicin delivery. *J. Mater. Chem. B,* **2013**, *1*, 6596–6607.

144. Peng, K.Y.; Wang, S.W.; Hua, M.Y.; Lee, R. Amphiphilic photocleavable block copolymers based on monomethyl poly(ethylene glycol) and poly(4-substituted-ε-caprolactone): synthesis, characterization, and cellular uptake. *RSC Adv.*, **2013**, *3*, 18453–18463.

145. McNamee, K. P.; Pitet, L. M.; Knauss, D. M. Synthesis, assembly, and cross-linking of polymer amphiphiles in situ: polyurethane–polylactide core–shell particles. *Polym. Chem.*, **2013**, *4*, 2546–2555.

146. Danquah, M.; Fujiwara, T.; Mahato, R. I. Self-assembling methoxy poly(ethylene glycol)-b-poly(carbonate-co-L-lactide) block copolymers for drug delivery. *Biomaterials* 2010, *31*, 2358–2370.

Captions:

Figure 1 Optical micrograph of PLLA16k-b-PEO5k copolymer films crystallized at (a) 90, (b) 100 (c)110, (d) 115, (e) 120, and (f) 125 ℃, from the melt. The bar corresponds to 100 μm. (Polym. Bull. 2011, 67, 885–902)

Figure 2 Morphological evolution of melt-crystallized PLLA-PEO diblock copolymer as a function of crystallization temperature.

Figure 3 Schematic representation of chain folding and domain spacing of PLLA block and amorphous PEO at low (a, 110 ℃) and high (b, 130 ℃) crystallization temperatures.

Figure 4 Optical micrographs in PLLA30k-b-PEO5k crystallized at (a) 120, (b) 130, (c) 130 ℃. (J. Poly. Sci. Part B: Poly. Phys. 2008, 46, 1400-1411.)

Figure 5 A series of AFM height images and cross-sectional profile data showing the crystallization process of LA505EG505 diblock copolymer. (a) annealed at 129 °C for 1592 s, (b) 2610 s; (c) 3897 s; (d) at 35 °C, the black arrows indicate the PEG crystal that formed at the edge of PLLA crystal; (e) annealed at 35 °C for 1085 s; (f) for 2878 s. (Macromolecules 2007, 40, 2791-2797)

Figure 6 POM images (a′) with and (a) without compensator, and (b) PCM images of LA5kEG5k obtained at 30 °C for different times: (a1 a1′and b1) 0 min; (a2) and (a2′) 1.3 min; (a3) 1.6 min, (b2) 2 min, (b3) 2.5 min, (a3′) 3 min, (a4′) 3.2 min, (a4) 3.3 min, and (b4) 3.5 min. The first-order red plate (λ = 530 nm) was used as compensator. (Macromolecules 2012, 45, 4254−4261)

Figure 7. Real-time POM micrographs of PEG50-PCL50. The specimen was melted at 80 °C for 5 min and then quenched to 38°C at 40 °C/min. (Biomacromolecules 2006, 7, 252 258)

Figure 8 Simultaneous (a) SAXS and (b) WAXS profiles collected during isothermal

crystallisation of PEO5k-PCL5k at 40 ℃ [90]. (Eur. Phys. J. E , 2008, 27, 357–364)

Figure 9 AFM height (left) images and phase (right) images of (a) PEG5000, (b) PCL8000, and (c) PEG5000 PCL5000. (Macromolecules 2006, 39, 3717 3719)

Figure 10. Lamellar crystals of L60C40 (PLLA-PCL) obtained from isothermal crystallizations performed at (a, b) 80 ℃, (c, d) 70 ℃, (e, f) 65 ℃, and electron diffraction pattern (65 ℃) of {110} growth faces (indicated by black dashed and white dotted lines). The inset b* axes for PCL and b PLLA crystals are labled in the electron diffraction pattern. (Polymer 2011, 52, 5166-5177)

Figure 11 (a) Projections along the helical axis of a 103 helical conformation of PLLA. (b1) Projections along the helical axis of a 31 helical conformation of sc-PLA (left: PLLA, right: PDLA).(b2) Projections perpendicular to the helical axis of a 31 helical conformation of sc-PLA (left: PLLA, right: PDLA). (b3) Crystal diagram of sc-PLA. (Journal of Macromolecular Science R, Part C: Polymer Reviews, 2009, 49, 107–140.)

Figure 12 (a) DSC curves and (b)WAXD profiles of the melt-polycondensates (prepolymers), melt-blend (blended at 170–250◦C for 5–20 min), and solid-state polycondensate (sb-PLA). (Macromol. Biosci. 2005, 5, 21–29)

Figure 13 Thermograms of stereo multiblock poly(lactic acid)s (MB) and stereo diblock poly(lactic acid) (DB) polymers and blend isothermally crystallized from the melt at different T_{cs}. (J. Appl. Polym. Sci. 2013, 129, 2502–2517)

Figure 14 Final spherulitic morphologies of PES-PEG multiblock copolymers

obtained at different crystallization temperatures: (A) PBS at 90 °C, (B) PES at 60 °C, (C) E47B46 at 90 °C, (D) E47B46 at 60 °C, (E) E54B51 at 90 °C, (F) E54B51 at 60 °C. (Polym. Chem., 2012, 3, 399–408)

Figure 15 AFM images of crystallized 6-armed PCL and 6-armed PCL-PLLA block copolymers. (Journal of Polymer Science: Part A: Polymer Chemistry 2010, *48*, 5063–5071.)

Figure 16 POM of (a) PCL, (b) N3-PCL-N3, (c) PLLA-b-(N3A)PCL-(N3-)-b-PLLA, (d) PLLA-b-(PDMAEMA-b-)-PCL(-b-PDMAEMA)-b-PLLA . (J Polym Sci Part A: Polym Chem 2012, 50, 2541–2552)

Figure 17 Morphologies of PLLA16k-b-PEO5k copolymer thin films crystallized at 110 ℃. Film thickness: (a) ~400 nm, (b) 220 nm, (c) 115 nm. The bar corresponds to 100 μm. (Langmuir, 2009, 25(22), 13125–13132.)

Figure 18 AFM height (left) and phase (right) images of PLLA16k-b-PEO5k copolymer thin films. (Langmuir, 2009, 25(22), 13125–13132.)

Figure 19 AFM height images of PEO(4k)-b-PCL(20k) films crystallized at room temperature at film thicknesses of (a) 14, (b) 10 nm. The bar corresponding 2 μm. (Polymer 52 (2011) 2085-2093).

Figure 20 AFM image of stereocomplex PM composed of an equimolar mixture of PEG-b-PDLA72 and PEG-b-PLLA73. Imaging (Nano Lett., Vol. 5, No. 2, 315-319)

Fig. 21 TEM micrographs of EO45LA46EO113 aggregates: (a) polymersomes, (b and

c) combination and dispersion of polymersomes, and (d) nanotube stretched from polymersomes.(Nanoscale, 2013, 5, 9010–9017)

Figure 22 Schematic presentation of self-assembling aggregates from triblock copolymers: (a) polymersomes and (b) nanotubes. (Nanoscale, 2013, 5, 9010–9017)

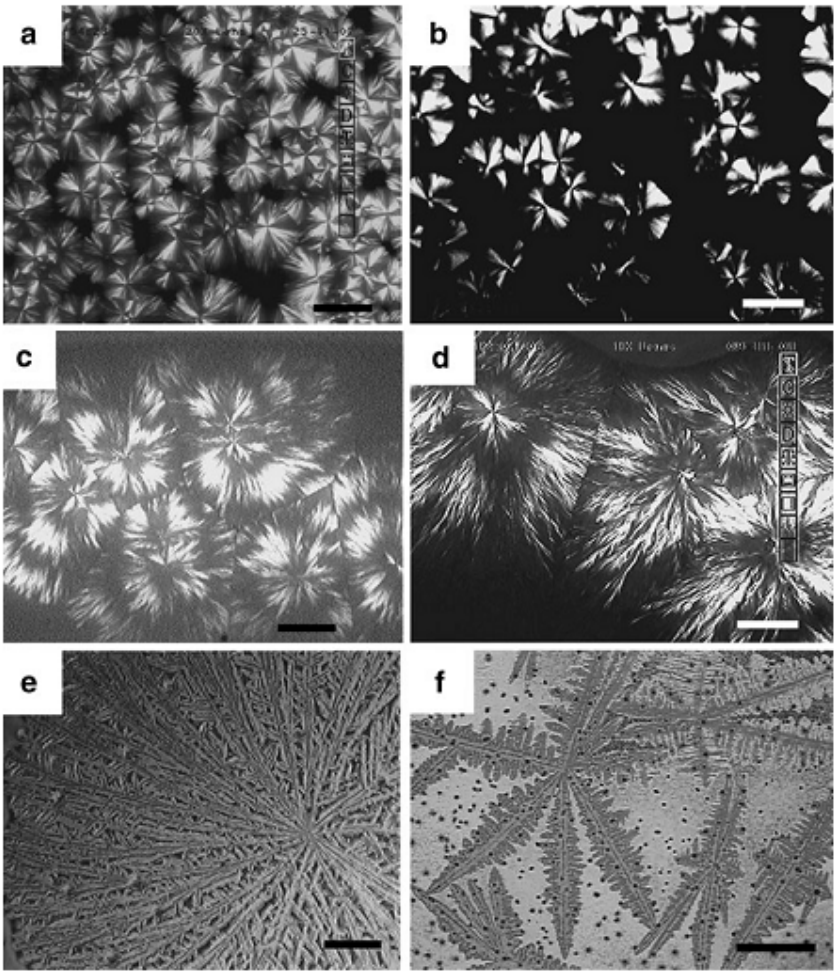

Figure 1 Optical microgrphs of PLLA16k-b-PEO5k copolymer films crystallized at (a) 90, (b) 100 (c)110, (d) 115, (e) 120, and (f) 125 ℃, from the melt. The bar corresponds to 100 μm. (Polym. Bull. 2011, 67, 885–902)

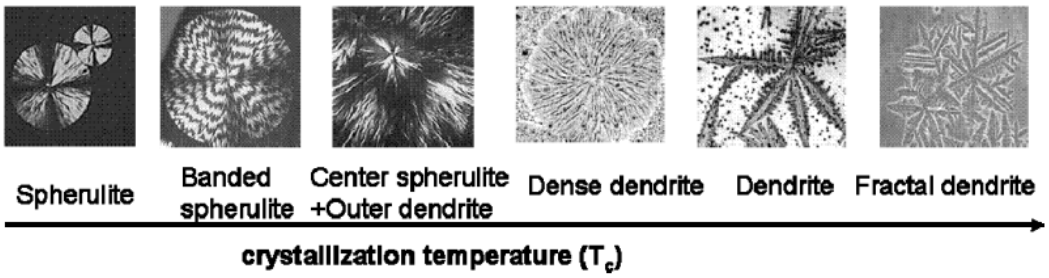

Figure 2 Morphological evolution of melt-crystallized PLLA-PEO diblock copolymer as a function of crystallization temperature.

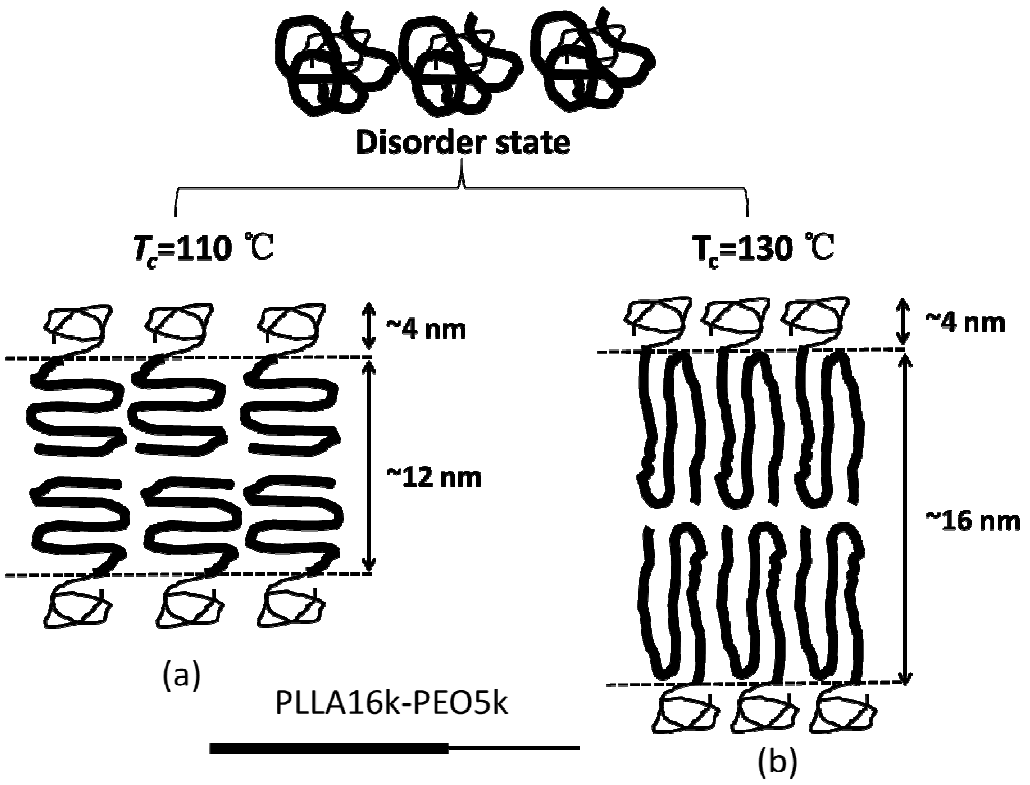

Figure 3 Schematic representation of chain folding and domain spacing of PLLA block and amorphous PEO at low (a, 110 ℃) and high (b, 130 ℃) crystallization temperatures.

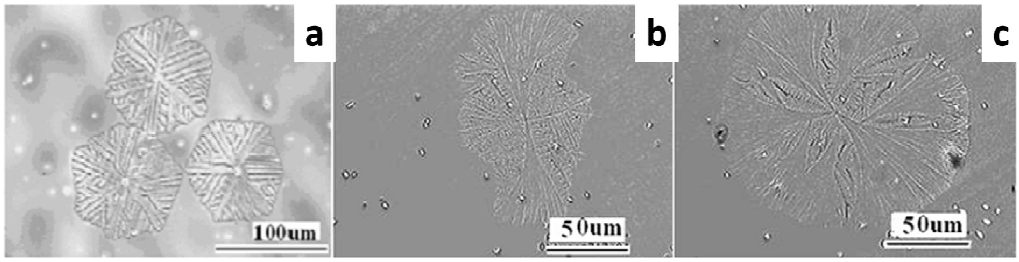

Figure 4 Optical micrographs in PLLA30k-b-PEO5k crystallized at (a) 120, (b) 130, (c) 130 ℃. (J. Poly. Sci. Part B: Poly. Phys. 2008, 46, 1400-1411.)

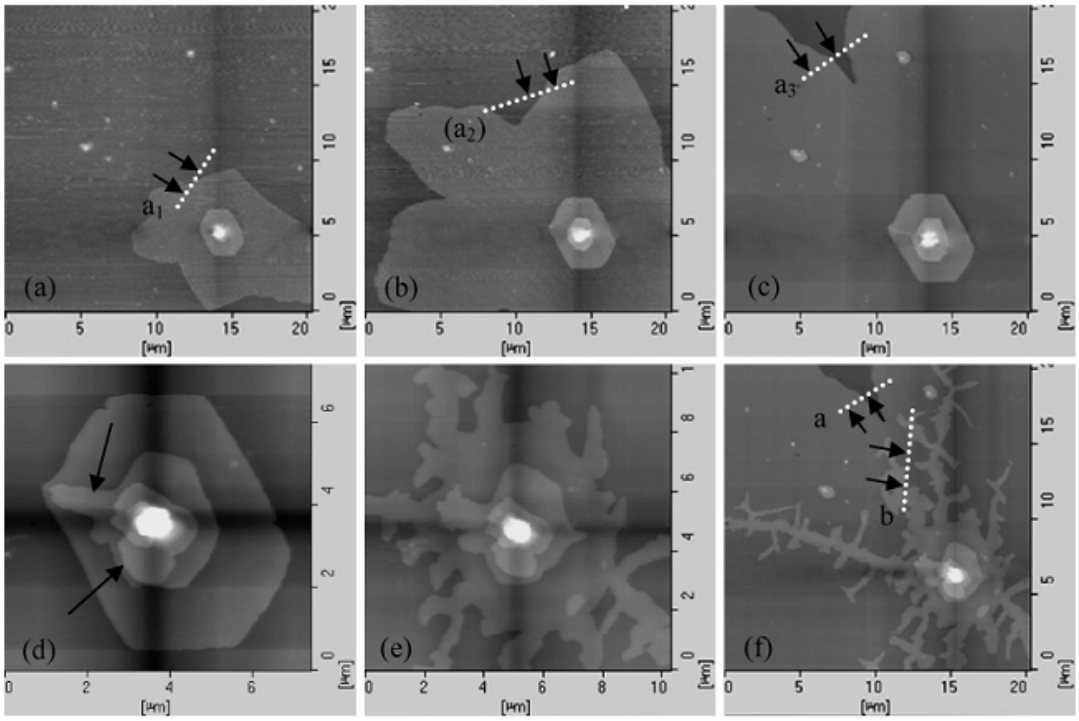

Figure 5 A series of AFM height images and cross-sectional profile data showing the crystallization process of LA505EG505 diblock copolymer. (a) annealed at 129 °C for 1592 s, (b) 2610 s; (c) 3897 s; (d) at 35 °C, the black arrows indicate the PEG crystal that formed at the edge of PLLA crystal; (e) annealed at 35 °C for 1085 s; (f) for 2878 s. (Macromolecules 2007, 40, 2791-2797)

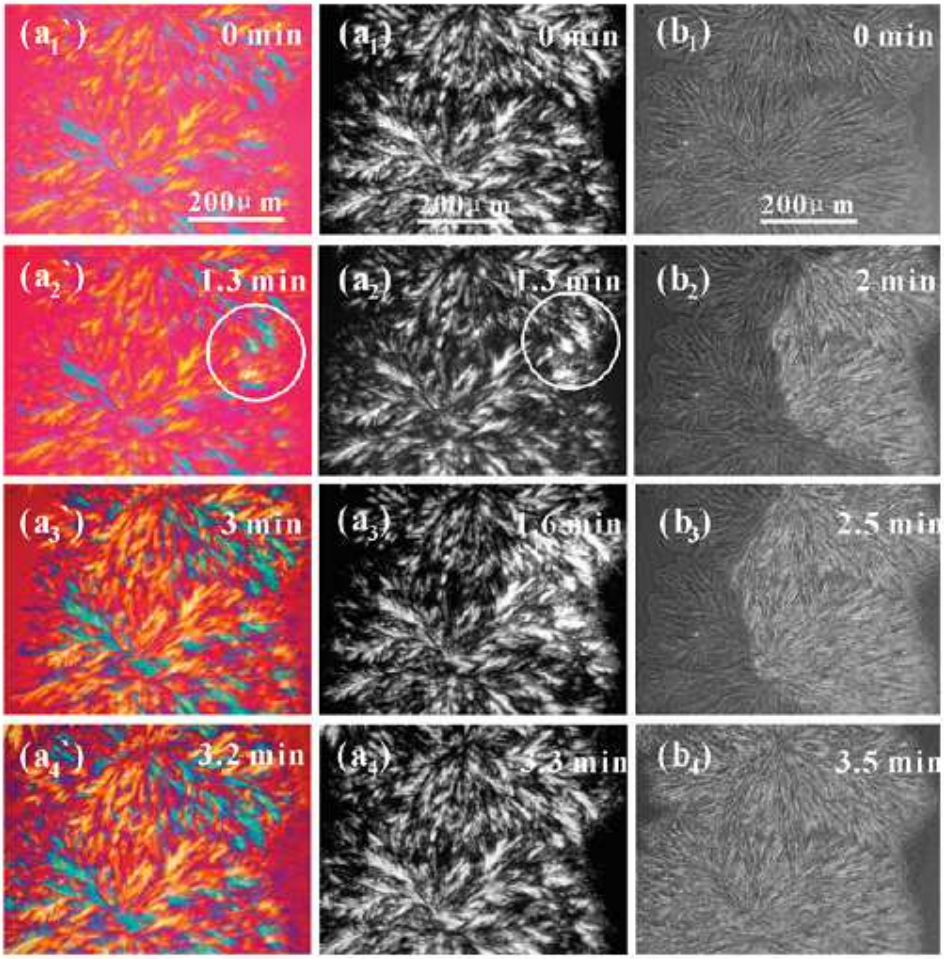

Figure 6 POM images (a′) with and (a) without compensator, and (b) PCM images of LA5kEG5k obtained at 30 °C for different times: (a1 a1′and b1) 0 min; (a2) and (a2′) 1.3 min; (a3) 1.6 min, (b2) 2 min, (b3) 2.5 min, (a3′) 3 min, (a4′) 3.2 min, (a4) 3.3 min, and (b4) 3.5 min. The first-order red plate (λ = 530 nm) was used as compensator. (Macromolecules 2012, 45, 4254−4261)

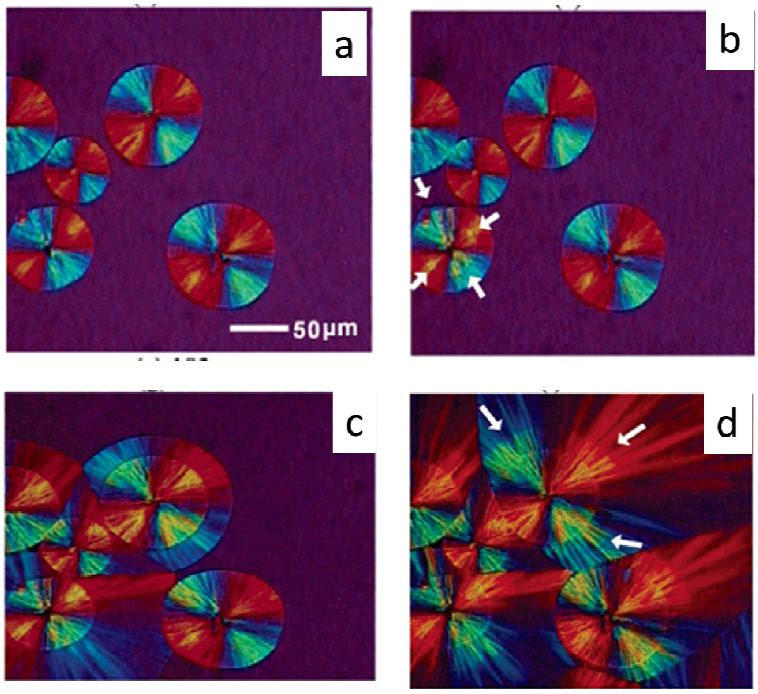

Figure 7. Real-time POM micrographs of PEG50-PCL50. The specimen was melted at 80 °C for 5 min and then quenched to 38°C at 40 °C/min. (Biomacromolecules 2006, 7, 252 258)

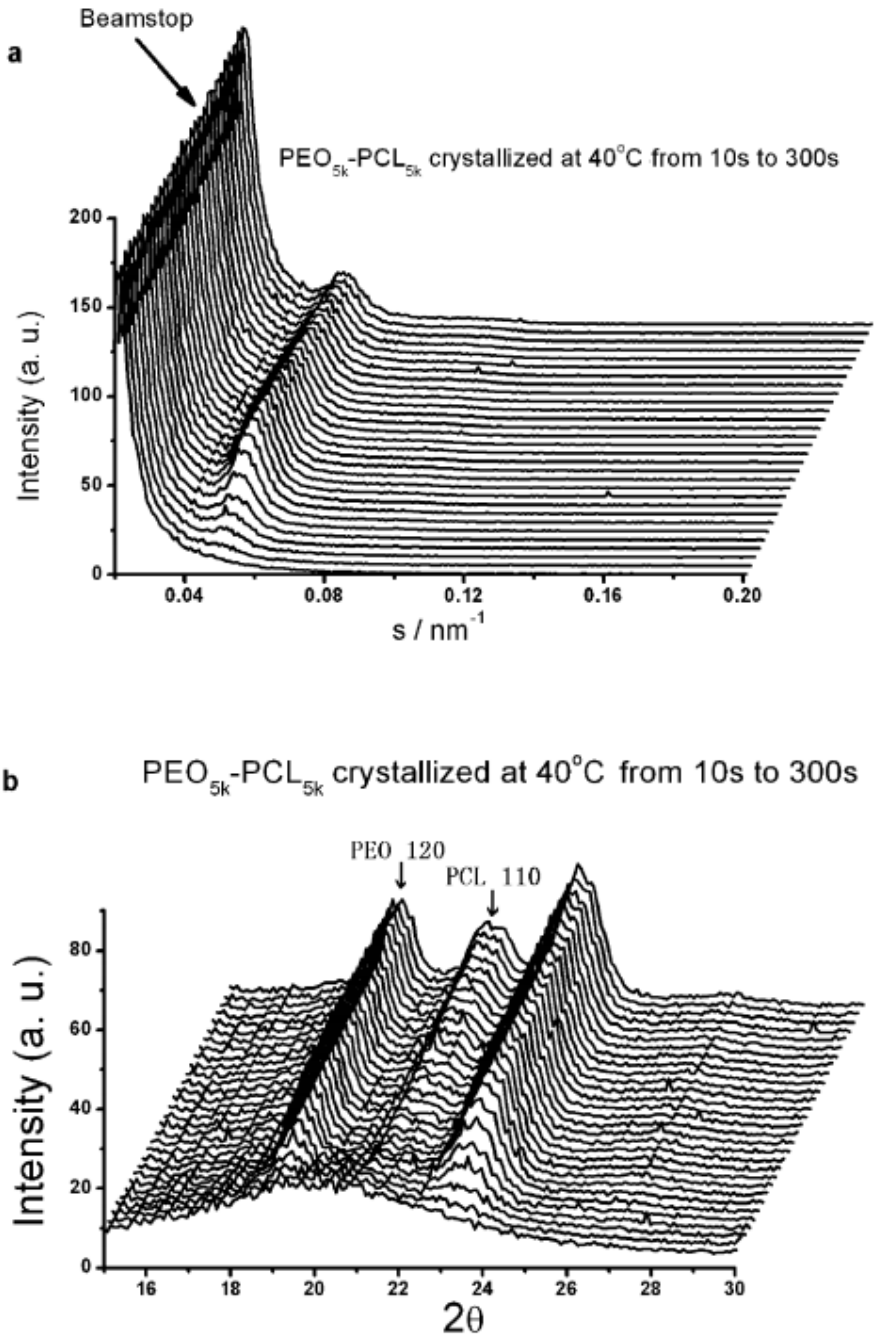

Figure 8 Simultaneous (a) SAXS and (b) WAXS profiles collected during isothermal crystallisation of PEO5k-PCL5k at 40 ℃. (Eur. Phys. J. E , 2008, 27, 357–364)

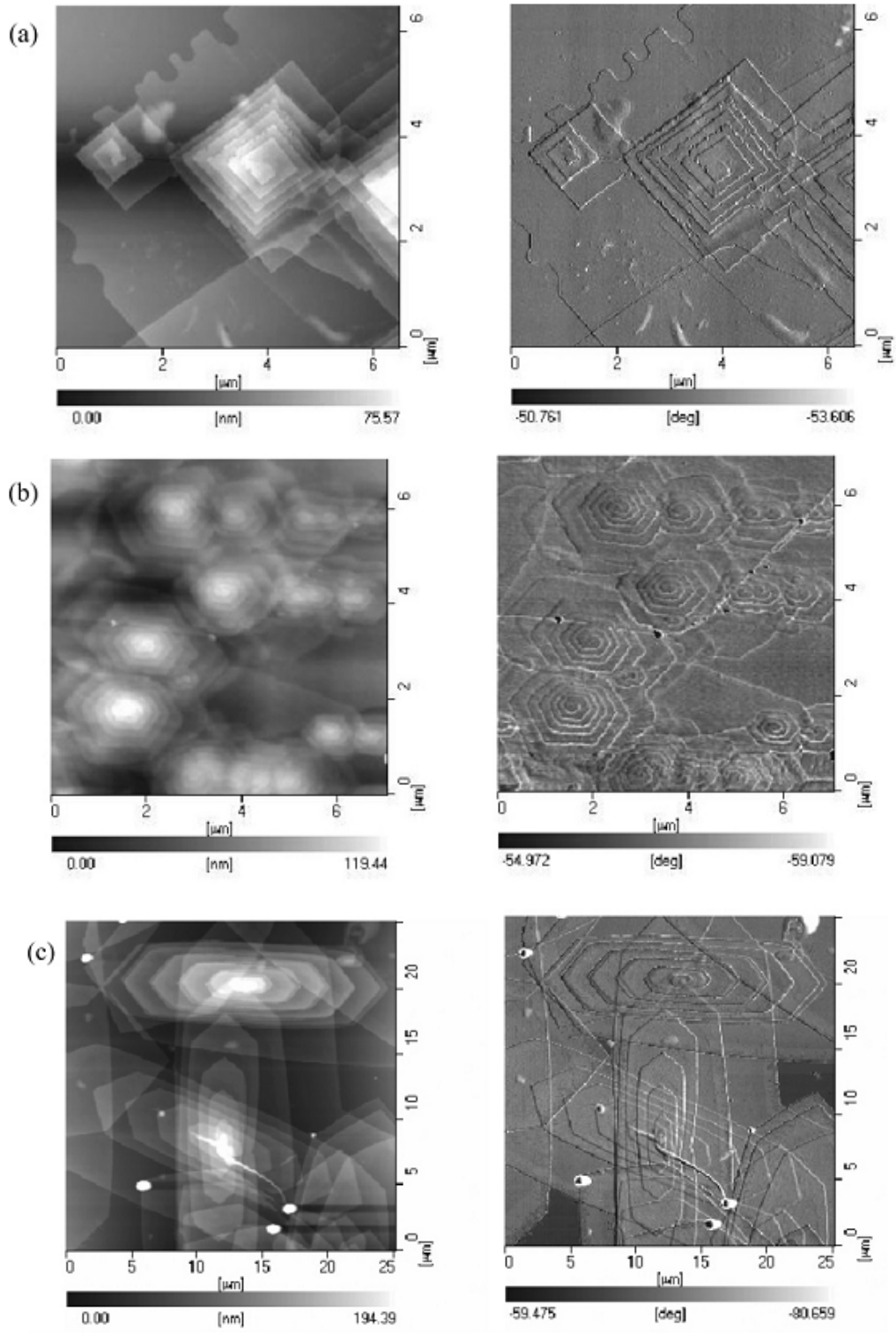

Figure 9 AFM height (left) images and phase (right) images of (a) PEG5000, (b) PCL8000, and (c) PEG5000 PCL5000. (Macromolecules 2006, 39, 3717 3719)

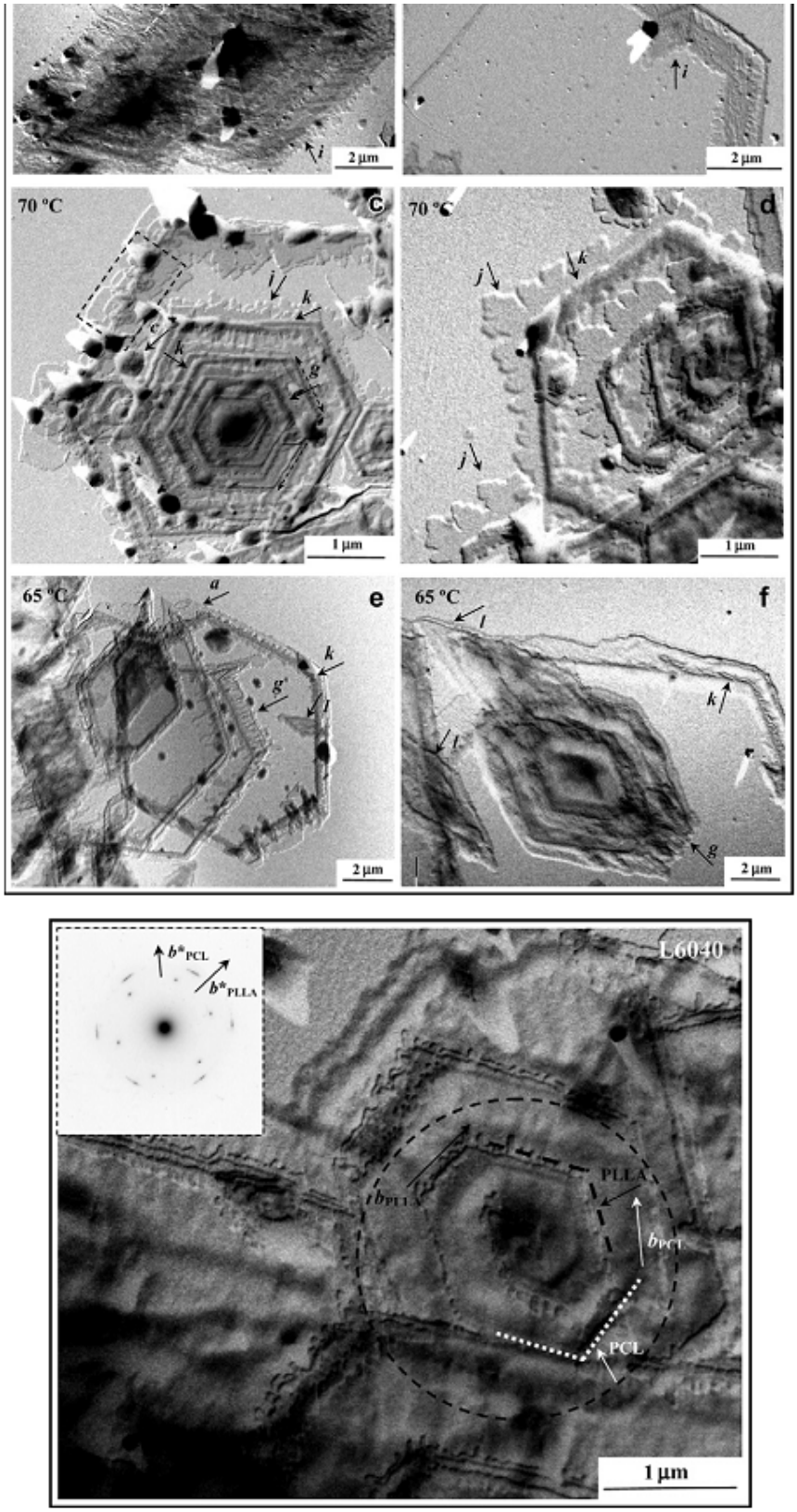

Figure 10. Lamellar crystals of L60C40 (PLLA-PCL) obtained from isothermal

crystallizations performed at (a, b) 80 ℃, (c, d) 70 ℃, (e, f) 65 ℃, and electron diffraction pattern (65 ℃) of {110} growth faces (indicated by black dashed and white dotted lines). The inset b* axes for PCL and b PLLA crystals are labled in the electron diffraction pattern. (Polymer 2011, 52, 5166-5177)

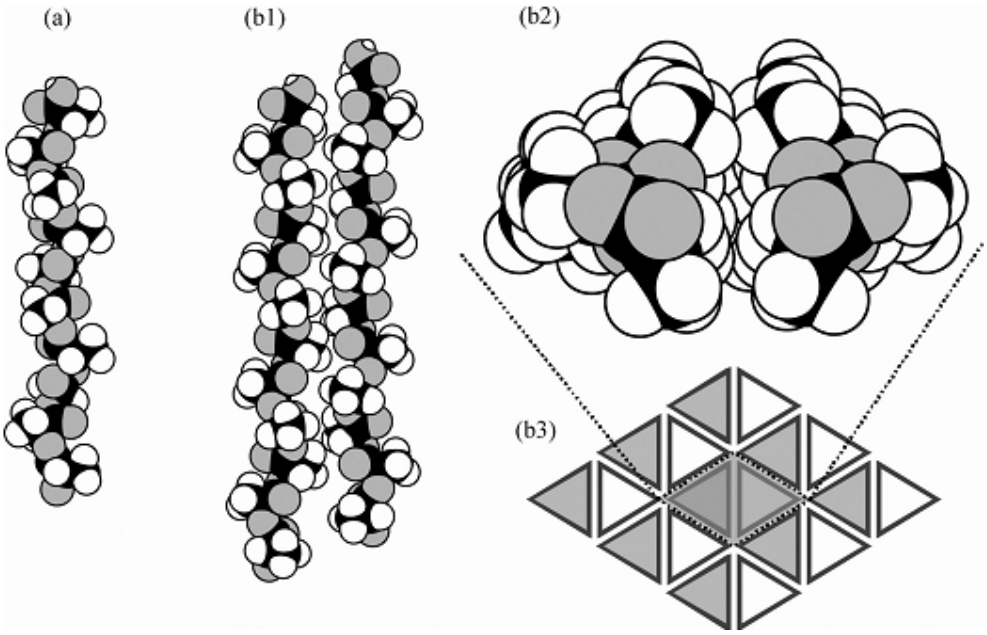

Figure 11 (a) Projections along the helical axis of a 103 helical conformation of PLLA. (b1) Projections along the helical axis of a 31 helical conformation of sc-PLA (left: PLLA, right: PDLA).(b2) Projections perpendicular to the helical axis of a 31 helical conformation of sc-PLA (left: PLLA, right: PDLA). (b3) Crystal diagram of sc-PLA. (Journal of Macromolecular Science R, Part C: Polymer Reviews, 2009, 49, 107–140.)

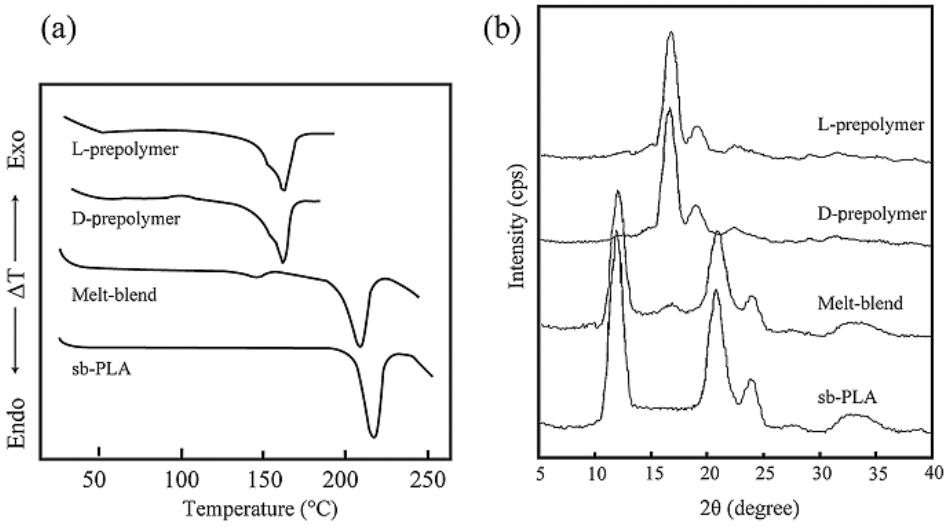

Figure 12 (a) DSC curves and (b)WAXD profiles of the melt-polycondensates (prepolymers), melt-blend (blended at 170–250◦C for 5–20 min), and solid-state polycondensate (sb-PLA). (Macromol. Biosci. 2005, 5, 21–29)

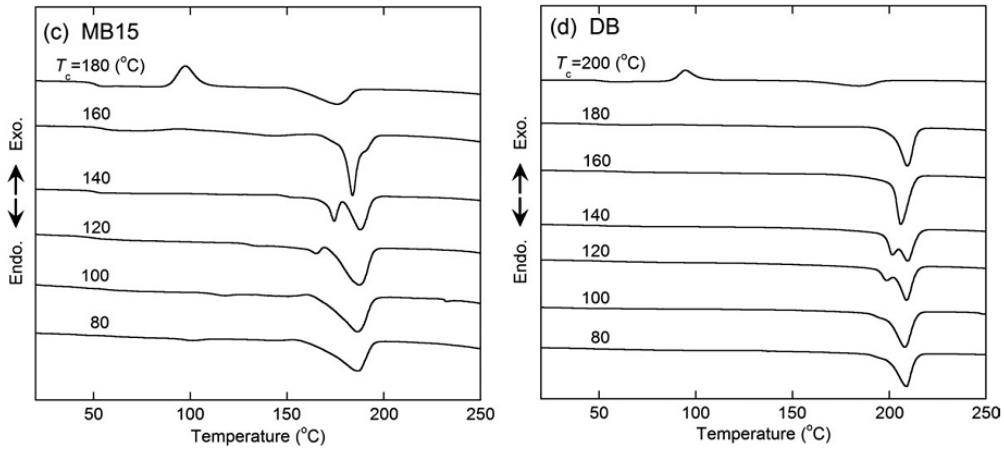

Figure 13 Thermograms of stereo multiblock poly(lactic acid)s (MB) and stereo diblock poly(lactic acid) (DB) polymers and blend isothermally crystallized from the melt at different T_{cs}. (J. Appl. Polym. Sci. 2013, 129, 2502–2517,)

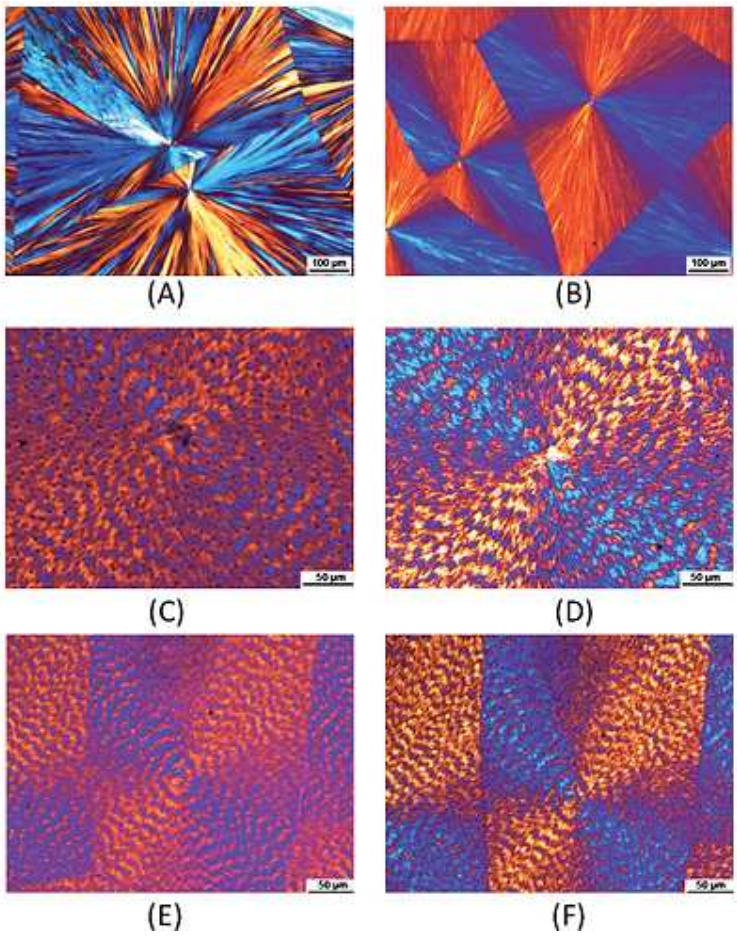

Figure 14 Final spherulitic morphologies of PES-PEG multiblock copolymers obtained at different crystallization temperatures: (A) PBS at 90 °C, (B) PES at 60 °C, (C) E47B46 at 90 °C, (D) E47B46 at 60 °C, (E) E54B51 at 90 °C, (F) E54B51 at 60 °C. (Polym. Chem., 2012, 3, 399–408)

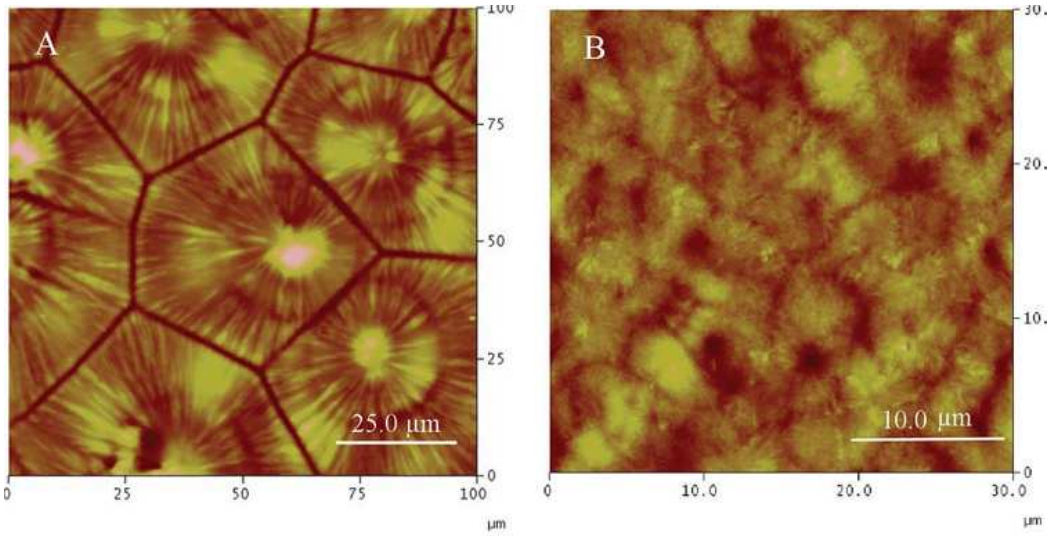

Figure 15 AFM images of crystallized 6-armed PCL and 6-armed PCL-PLLA block copolymers. (Journal of Polymer Science: Part A: Polymer Chemistry 2010, *48*, 5063–5071.)

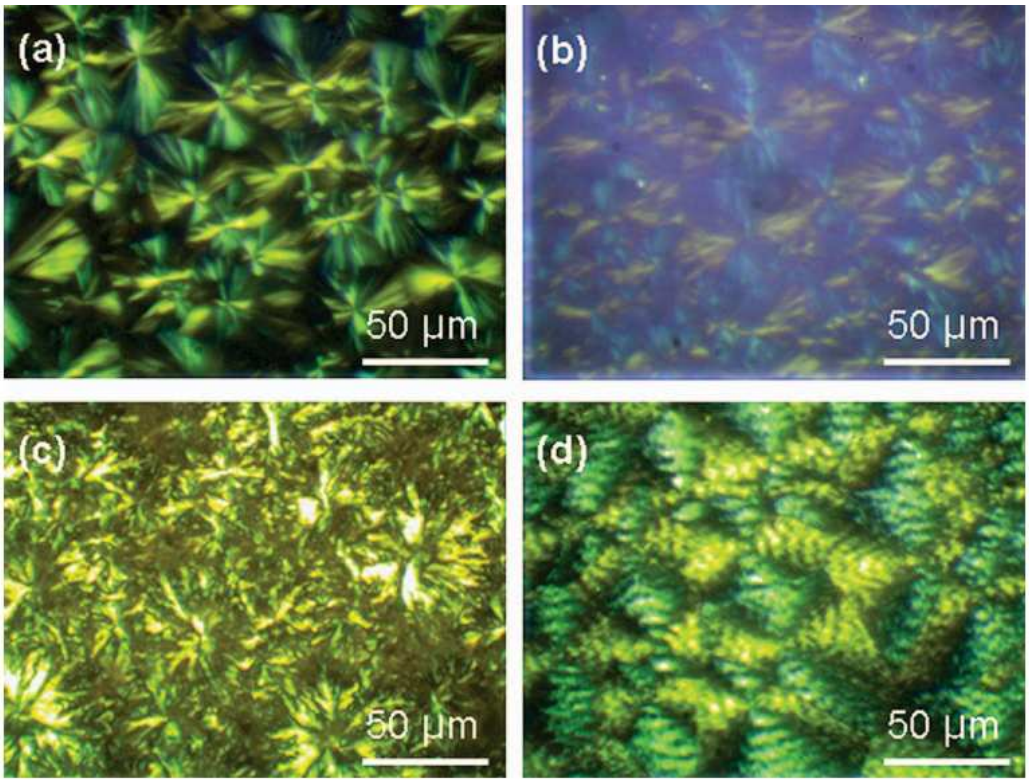

Figure 16 POM of (a) PCL, (b) N3-PCL-N3, (c) PLLA-b-(N3A)PCL-(N3-)-b-PLLA, (d) PLLA-b-(PDMAEMA-b-)-PCL(-b-PDMAEMA)-b-PLLA . (J Polym Sci Part A: Polym Chem 2012, 50, 2541–2552)

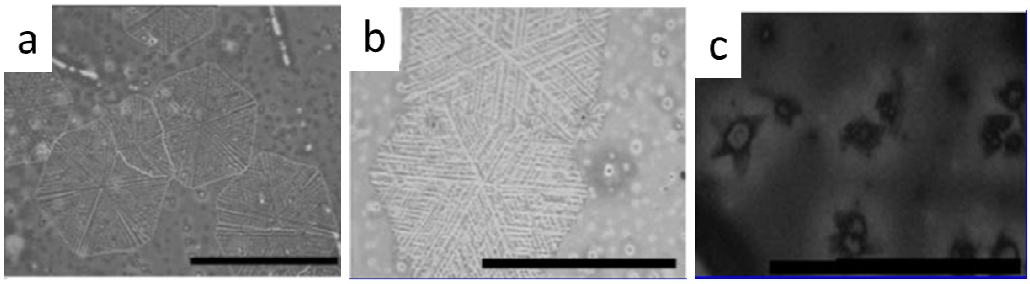

Figure 17 Morphologies of PLLA16k-b-PEO5k copolymer thin films crystallized at 110 ℃ from melt. Film thickness: (a) ~400 nm, (b) 220 nm, (c)115 nm. The bar corresponds to 100 μm. (Langmuir, 2009, 25(22), 13125–13132.)

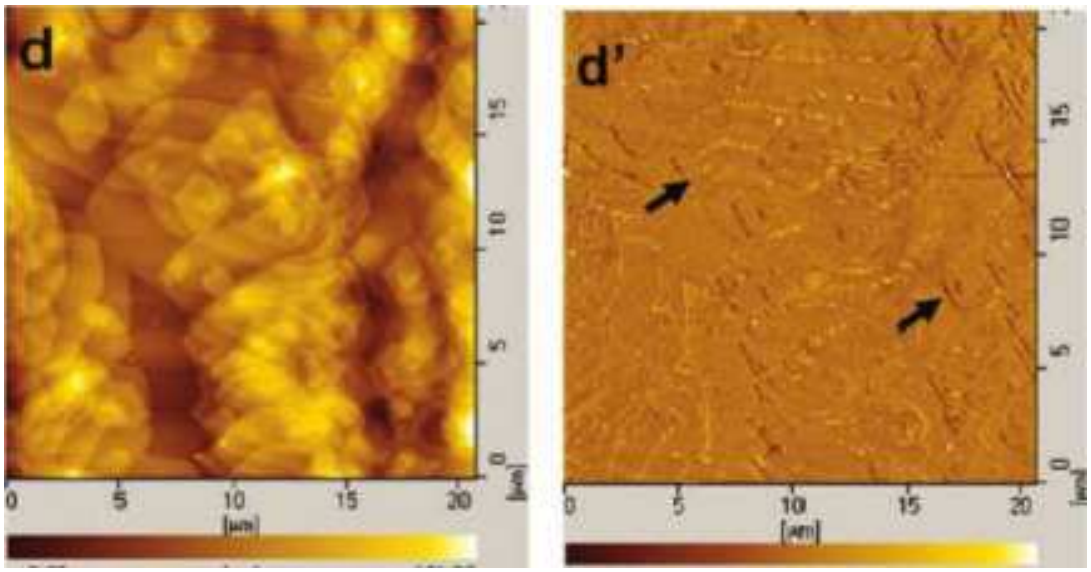

Figure 18 AFM height (left) and phase (right) images of PLLA16k-b-PEO5k copolymer thin films. (Langmuir, 2009, 25(22), 13125–13132.)

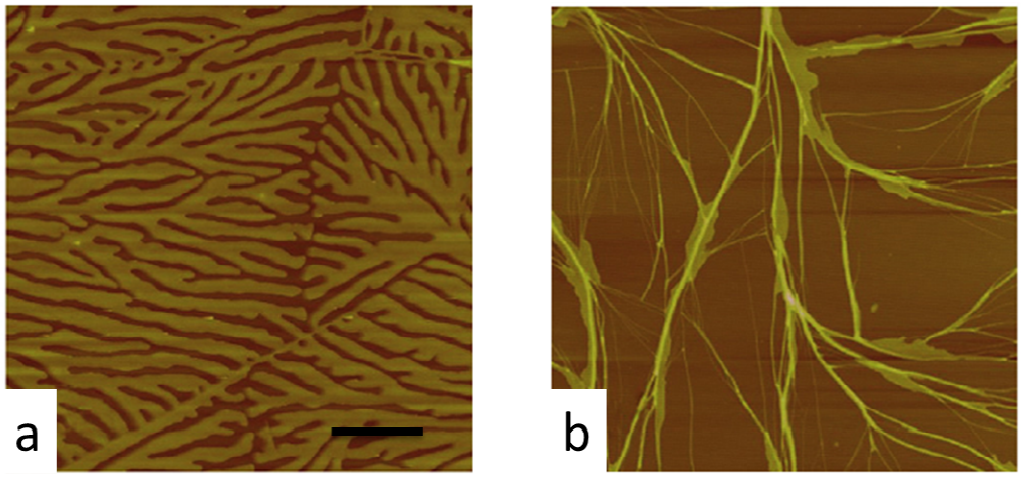

Figure 19 AFM height images of PEO(4k)-b-PCL(20k) films crystallized at room temperature at film thicknesses of (a) 14, (b) 10 nm. The bar corresponding 2 μm. (Polymer 2011, 52, 2085-2093).

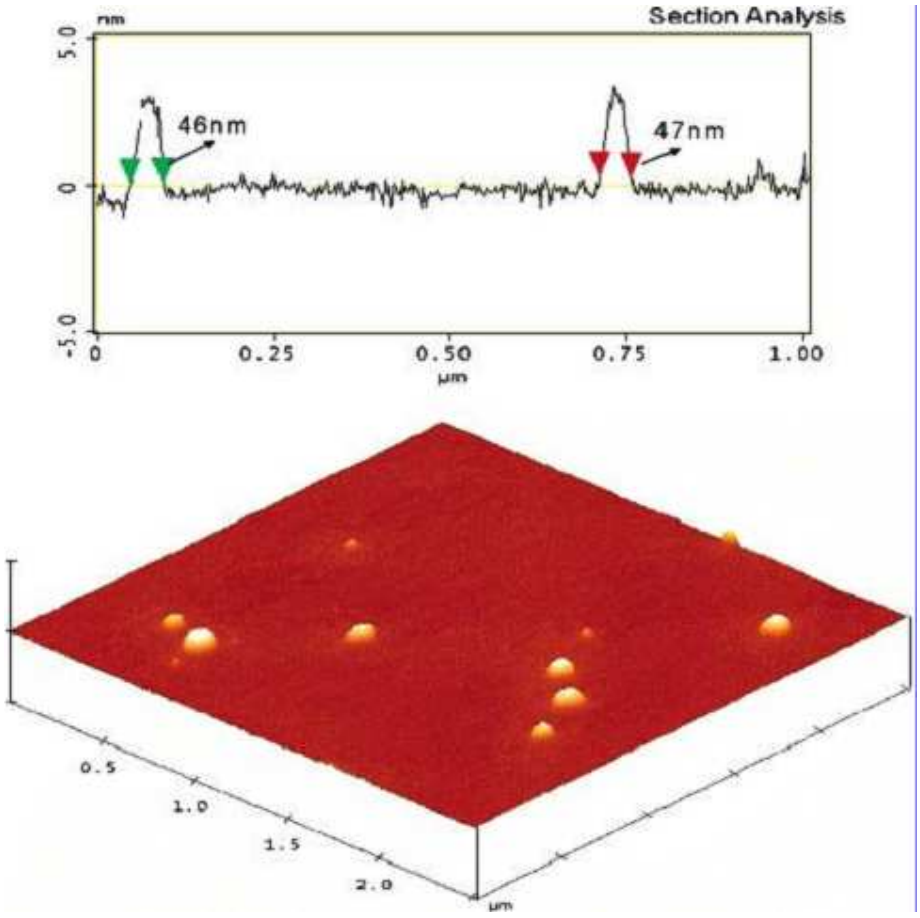

Figure 20 AFM image of stereocomplex PM composed of an equimolar mixture of PEG-b-PDLA72 and PEG-b-PLLA73. Imaging (Nano Lett., 2005, Vol. 5, No. 2, 315-319)

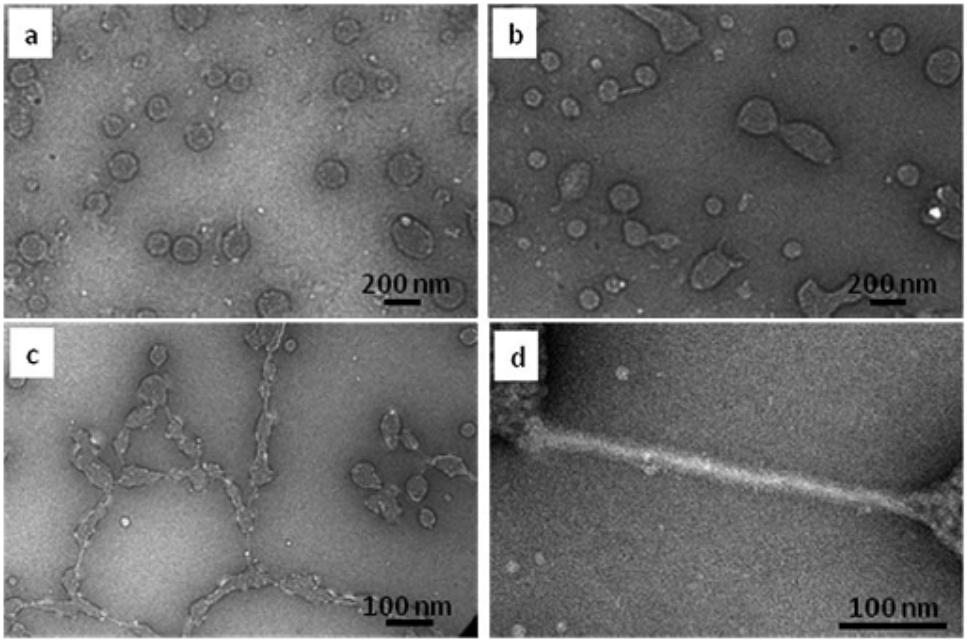

Fig. 21 TEM micrographs of EO45LA46EO113 aggregates: (a) polymersomes, (b and c) combination and dispersion of polymersomes, and (d) nanotube stretched from polymersomes.(Nanoscale, 2013, 5, 9010–9017)

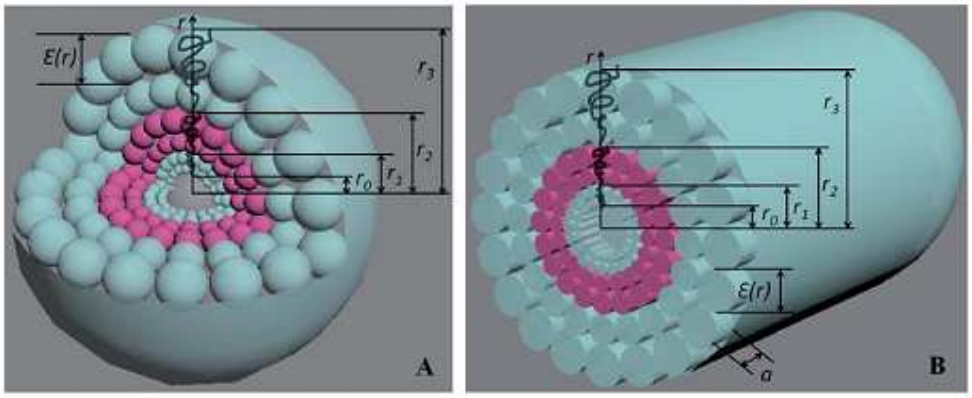

Figure 22 Schematic presentation of self-assembling aggregates from triblock copolymers: (a) polymersomes and (b) nanotubes. (Nanoscale, 2013, 5, 9010–9017)